Eur. Phys. J. Special Topics **229**, 2497–2526 (2020)

https://doi.org/10.1140/epjst/e2020-000014-5

THE EUROPEAN PHYSICAL JOURNAL SPECIAL TOPICS

Review

# Exact solutions of mean-field plus various pairing interactions and shape phase transitions in nuclei

Feng Pan[1,2,a], Xin Guan[1], Lian-Rong Dai[1], Yu Zhang[1], and Jerry P. Draayer[2]

[1] Department of Physics, Liaoning Normal University, Dalian 116029, P.R. China
[2] Department of Physics and Astronomy, Louisiana State University, Baton Rouge, LA 70803-4001, USA

Received 1 February 2020 / Accepted 28 August 2020
Published online 23 October 2020

**Abstract.** The exact solutions of either spherical or deformed mean-field plus various types of pairing models are briefly reviewed. It is shown that, besides the standard pairing model, there are several special types of pairing interaction that can be solved exactly. In comparison to the standard pairing, the results of several pairing-driven quantities, such as pairing excitation energies, even–odd mass differences, the moment of inertia, etc., show that these types of pairing interaction can indeed be used to describe pairing correlations in nuclei either more accurately or efficiently. Moreover, the shape phase transitional behaviors of nuclei described by the consistent-$Q$ formalism of the interacting boson model are summarized.

## 1 Introduction

Nuclear pairing correlation, as an important part of the residual interactions necessary to augment any nuclear mean-field theory, represents one of the main and longstanding pillars of current understanding of nuclear structure [1]. For example, the pairing interaction of the nuclear shell model plays a key role to reproduce low-energy spectroscopic properties of nuclei, such as binding energies, odd-even effects, single-particle occupancies, excitation spectra, and moments of inertia, etc. [2,3]. Bohr, Mottelson, Pines, and Belyaev were the first to introduce the Bardeen–Cooper–Schrieffer (BCS) theory for superconductivity in condensed matter [4] to descriptions of pairing phenomena in nuclei [2,5]. Though the BCS and the more refined Hartree–Fock–Bogolyubov (HFB) approximations provide simple and clear pictures in demonstrating pairing correlations in nuclei [2,6,7], tremendous efforts have been made in finding accurate solutions to the problem [8–14] to overcome serious drawbacks in the BCS and the HFB, such as spurious states, nonorthogonal solutions, etc. resulting from particle number-nonconservation effects in these approximations [9,10,14–16]. Driven by the importance of having exact solutions of either spherical or deformed mean-field plus the standard pairing Hamiltonian, much attention and progress, building on Richardson and Gaudin's early work [17–21] and

[a] e-mail: daipan@dlut.edu.cn

extensions to it based on the Bethe ansatz, have been made [22–32]. For all these algebraic Bethe ansatz approaches, the solutions are provided by a set of highly non-linear Bethe–Gaudin–Richardson equations (BGREs). Though these applications demonstrate that the pairing problem is exactly solvable, solutions of these BGREs are not easy and normally require extensive numerical work, especially when the number of levels and valence pairs are large [27]. This limits the applicability of the method to relatively small systems. However, it has been shown recently that the set of BGREs for the standard pairing case can be solved relatively easily by using the extended Heine–Stieltjes polynomial approach [33–35]. Since solutions of the standard pairing model can be obtained from zeros of the associated extended Heine–Stieltjes polynomials, the approach can be applied to study the model with more pairs over a larger number of single-particle levels.

Moreover, if nuclear pairing interaction is restricted to nearest levels in a deformed mean-field theory, it leads to a simply solvable hard-core Bose–Hubbard model Hamiltonian, which may also be suitable to describe well-deformed nuclei [36–38]. Later on, the Nilsson mean-field plus an extended pairing model was also proposed to describe deformed nuclei [39], which includes pairing interactions among valence pairs in different levels up to infinite order. It has been shown that the extended pairing model can be regarded as the standard pairing Hamiltonian at a first-order approximation, namely, only the lowest energy eigenstate described by the Racah quasi-spin formulism of the standard pairing interaction is taken into consideration, and the results thus display similar pair structures to those in the low-lying states of the standard pairing model [40]. The advantage of the model lies in the fact that it can also be solved exactly and more easily than the standard pairing model, especially when both the number of valence nucleon pairs and the number of single-particle levels are large, which, therefore, is more suitable to describe well-deformed nuclei [41–43].

In quantum many-body systems, such as atomic nuclei, quantum phase transition (QPT) has been one of the interesting and important phenomena, which occurs at zero temperature in the thermodynamic limit [44]. In nuclei, quantum phase is often referred to as the shape (phase) of a nucleus. Typical shape is of spherical (vibrational), indefinite triaxial ($\gamma$-unstable), or axially deformed (rotational) type, which is manifested by the collective model [45] and the interacting boson model (IBM) [46]. Shape (phase) evolution can be observed at ground state or low-lying states of nuclei along a chain of isotopes or isotones, in which noticeable changes in physical quantities or called effective order parameters, such as energy ratios, B(E2) ratios, and binding energy related quantities, are not only predicted in theory, but also experimentally observed [47,48]. Besides the collective model and shell model descriptions, as is well known, the interacting boson model (IBM) has been proven to be very successful in the description of both collective valence shell [46] and multi-particle–hole [49–51] excitations in nuclei. Most noticeably, the IBM Hamiltonian without configuration mixing can be solved analytically in the U(5) (vibrational), O(6) ($\gamma$-unstable), SU(3), or $\overline{\mathrm{SU}}(3)$ (rotational) limits [46], and the U(5)–O(6) transitional case [52], with which the shape (phase) evolution along a chain of isotopes or isotones can be clearly demonstrated.

In the following sections, we briefly review either spherical or deformed mean-field plus the standard pairing, the special separable and non-separable pairing, the nearest level pairing, and the extended pairing models. Application of these models to describe pairing excitations, even–odd mass differences, the moment of inertia, and possible phase transition will also be presented. Then, the shape phase transitional behaviors of nuclei described by the IBM are presented. A brief summary is given in the final section.

## 2 Mean-field plus pairing models and their applications

Once the mean-field contribution is determined by using the HF method or described by an effective single-particle potential, which can be expressed as diagonal one-body terms of a nuclear Hamiltonian in a complete or truncated subspace of (valence) nucleons, there are several important residual interactions to be considered. The pairing interaction among (valence) nucleon pairs is one of them. In the following, only pairing interaction among like-nucleon pairs is considered. Thus, the general spherical mean-field plus pairing Hamiltonian can be expressed as

$$\hat{H} = \sum_j \epsilon_j \hat{n}_j - \sum_{jj'} g_{jj'} S_j^+ S_{j'}^- = \sum_j \epsilon_j \hat{n}_j + \hat{H}_P, \tag{1}$$

where the sums run over given $j$-orbits of total number $p$, $\epsilon_j$ are nondegenerate single-particle energies generated from any spherical mean-field theory, $\hat{n}_j = \sum_m a_{jm}^\dagger a_{jm}$ is the number operator for (valence) like-nucleons in the $j$th level, $S_j^+ = \sum_m (-)^{j-m} \times a_{jm}^\dagger a_{j\,-m}^\dagger$ ($S_j^- = (S_j^+)^\dagger$) are pair creation (annihilation) operators, and $\{g_{jj'}\}$ are pairing interaction strengths among like-nucleon pairs, which, in general, are treated as adjustable parameters according to the binding energy and the low-lying excitation spectrum for a given nucleus. On the other hand, the deformed mean-field plus pairing Hamiltonian is written as

$$\hat{H} = \sum_i \varepsilon_i \hat{n}_i + \sum_{i,i'} G_{ii'} b_i^\dagger b_{i'}, \tag{2}$$

where $\{\varepsilon_i\}$ are a set of single-particle energies generated from any deformed mean-field theory, $b_i^\dagger = a_i^\dagger a_{\bar{i}}^\dagger$ and $b_i = a_{\bar{i}} a_i$, in which $a_i^\dagger$ is the $i$th level single-particle creation operator in the deformed basis, such as that of the Nilsson model, and $a_{\bar{i}}^\dagger$ the corresponding time-reversed state. In the following, some special cases of $\{g_{jj'}\}$ in the spherical basis or $\{G_{i'}\}$ in the deformed basis are considered, with which the Hamiltonian (1) can be solved exactly. The exact solutions of spherical mean-field plus various types of pairing will be discussed in Sections 2.1–2.4, while those of deformed mean-field plus nearest level pairing or extended pairing will be presented in Sections 2.5 and 2.6.

### 2.1 Mean-field plus standard pairing

The Hamiltonian of the standard pairing model (SPM) is given by

$$\hat{H} = \sum_j \epsilon_j \hat{n}_j - G \sum_{jj'} S_j^+ S_{j'}^- = \sum_j \epsilon_j \hat{n}_j + \hat{H}_P, \tag{3}$$

where $G > 0$ is the overall pairing strength, which is often adopted in many model calculations [3].

The $p$ copies of the local $SU(2)$ algebras with the generators $\{S_{j_t}^-,\ S_{j_t}^+,\ \hat{N}_{j_t}\}$ ($t = 1, 2, \ldots, p$), generate $p$ copies of SU(2) algebra satisfying the commutation relations

$$[\hat{N}_{j_t}/2,\ S_{j_{t'}}^-] = -\delta_{tt'} S_{j_t}^-,\ [\hat{N}_{j_t}/2,\ S_{j_{t'}}^+] = \delta_{tt'} S_{j_t}^+,\ [S_{j_t}^+,\ S_{j_{t'}}^-] = 2\delta_{tt'} S_{j_t}^0, \tag{4}$$

where $S^0_{j_t} = (\hat{N}_{j_t} - \Omega_t)/2$ with $\Omega_t = j_t + 1/2$. Let

$$S^+(x) = \sum_{t=1}^{p} \frac{1}{2\epsilon_{j_t} - x} S^+_{j_t}, \tag{5}$$

where $x$ is the (spectral) parameter to be determined. According to the commutation relations given in (4), we have

$$\left[ \sum_t \epsilon_{j_t} \hat{N}_{j_t},\ S^+(x) \right] = \sum_t \frac{2\epsilon_{j_t}}{2\epsilon_{j_t} - x} S^+_{j_t} = \sum_t S^+_{j_t} + x\, S^+(x), \tag{6}$$

$$[\hat{H}_{\rm P},\ S^+(x)] = G \sum_{t'} S^+_{j_{t'}} \sum_t \frac{2S^0_{j_t}}{2\epsilon_{j_t} - x} = G\, S^+\, \Lambda_0(x), \tag{7}$$

where $\Lambda_0(x) = \sum_t \frac{2S^0_{j_t}}{2\epsilon_{j_t} - x}$, $S^0_{j_t} = (N_{j_t} - \Omega_t)/2$,

$$\begin{aligned} [[\hat{H}_{\rm P},\ S^+(x)],\ S^+(y)] &= 2G \textstyle\sum_{t'} S^+_{j_{t'}} \sum_t \frac{1}{(2\epsilon_{j_t} - x)(2\epsilon_{j_t} - y)} S^+_{j_t} \\ &= S^+ \tfrac{2G}{x-y} \left( S^+(x) - S^+(y) \right), \end{aligned} \tag{8}$$

where $S^+ = \sum_{t'} S^+_{j_{t'}}$.

The Bethe–Gaudin–Richardson ansatz for $k$-pair eigenstates of (3) is written as [17–21]

$$|\xi; k; \nu\eta JM\rangle = \prod_{\rho=1}^{k} S^+(x^{(\xi)}_\rho) |\nu\eta JM\rangle, \tag{9}$$

where $x^{(\xi)}_1 \neq x^{(\xi)}_2 \neq \cdots \neq x^{(\xi)}_k$ is assumed, $\xi$ denotes the $\xi$th set of the solutions corresponding to the $\xi$th eigenstate of (3). If the seniority number of the $t$th orbit is $\nu_t$, the pairing vacuum states of the $p$ orbits are denoted as $|\nu_t \eta_t J_t M_t\rangle$ satisfying $S^-_{j_t} |\nu_{j_t} \eta_t J_t M_t\rangle = 0$, where $J_t$ and $M_t$ are the angular momentum quantum number and that of its third component, respectively, and $\eta_t$ is the multiplicity label needed to distinguish different possible ways of $\nu_t$ particles coupled to the angular momentum $J_t$. Thus, a pairing vacuum state of the system with the total seniority number $\nu = \sum_{t=1}^{p} \nu_t$ and the total angular momentum $J$ can be expressed as $|\nu\eta JM\rangle \equiv |\nu_1 \eta_1, \nu_2 \eta_2, \ldots, \nu_p \eta_p; (J_1 \otimes J_2 \otimes \cdots \otimes J_p), \eta, JM\rangle$, where $\eta$ is the outer-multiplicity label needed for the coupling of $J_1 \otimes J_2 \otimes \cdots \otimes J_p \downarrow J$. Thus, $|\nu\eta JM\rangle$ satisfies $S^-_{j_t} |\nu\eta JM\rangle = 0$ for $t = 1, 2, \ldots, p$, which is used in (9).

Using equations (6), (7), and (8), one can directly check that

$$\begin{aligned} \sum_t \epsilon_t\, \hat{N}_{j_t} |\xi; k; \nu\eta JM\rangle = &\ \textstyle\sum_i^k S^+ \prod_{\rho\,(\neq i)}^k S^+(x^{(\xi)}_\rho) |\nu\eta JM\rangle \\ &+ \left( \textstyle\sum_i^k x^{(\xi)}_i \right) \prod_\rho^k S^+(x^{(\xi)}_\rho) |\nu\eta JM\rangle \end{aligned} \tag{10}$$

and

$$\hat{H}_{\rm P}|\xi;k;\nu\eta JM\rangle = \sum_{i}^{k} G\Lambda_0(x_i^{(\xi)})\, S^+ \prod_{\rho\,(\neq i)}^{k} S^+(x_\rho^{(\xi)})|\nu\eta JM\rangle + \sum_{i}^{k}\sum_{i'\,(\neq i)}^{k} \frac{2G}{x_{i'}^{(\xi)} - x_i^{(\xi)}}\, S^+ \prod_{\rho\,(\neq i)}^{k} S^+(x_\rho^{(\xi)})|\nu\eta JM\rangle,$$

which leads to a set of Bethe–Gaudin–Richardson equations (BGREs) [17–21,28]:

$$1 - 2G\sum_{t}\frac{\rho_t}{x_i^{(\xi)} - 2\epsilon_{j_t}} - 2G\sum_{i'(\neq i)}^{k}\frac{1}{x_i^{(\xi)} - x_{i'}^{(\xi)}} = 0 \tag{11}$$

for $i = 1, 2, \ldots, k$, where the first sum runs over all $j$-levels and $\rho_t = -(\Omega_t - \nu_t)/2$. For each set of solution $\{x_1^{(\xi)}, \ldots, x_k^{(\xi)}\}$, the corresponding eigen-energy is given by

$$E_k^{(\xi)} = \sum_{t=1}^{p}\epsilon_{j_t}\nu_{j_t} + \sum_{i=1}^{k} x_i^{(\xi)}, \tag{12}$$

in which $\sum_{t=1}^{p}\epsilon_{j_t}\nu_{j_t}$ is contributed from particles in the pairing vacuum $|\nu\eta JM\rangle$.

As shown by Heine and Stieltjes, there is a one-to-one correspondence between a set of the BGREs and a set of orthogonal polynomials, called the extended Heine–Stieltjes polynomials [33,34]. Roots of these BGREs are zeros of the polynomials. Let $y(x)$ be a polynomial of degree $k$ satisfying the following second order Fuchsian equation:

$$A(x)y''(x) + B(x)y'(x) - V(x)y(x) = 0. \tag{13}$$

Here, $A(x) = \prod_{j=1}^{p}(x - 2\epsilon_j)$ is a polynomial of degree $p$, the polynomial $B(x)$ is given as

$$B(x)/A(x) = \sum_{j}\frac{2\rho_j}{x - 2\epsilon_j} - \frac{1}{G}, \tag{14}$$

$V(x)$ is called Van Vleck polynomial of degree $p-1$, which is determined according to equation (13). The polynomial $y(x)$ of degree $k$ with $k$ zeros $x_i$ may be expressed as

$$y(x) = \prod_{i=1}^{k}(x - x_i). \tag{15}$$

One can easily check that $y(x)$ satisfies

$$\frac{y''(x_i)}{y'(x_i)} = \sum_{j=1}^{k}\frac{2}{x_i - x_j}. \tag{16}$$

Equation (13) of $y(x)$ at zero $x_i$ leads to the BGREs shown in (11). The number of solutions should equal exactly to

$$\eta(p,k) = \sum_{q_1=0}^{-2\rho_1} \cdots \sum_{q_p=0}^{-2\rho_p} \delta_{q,k} \tag{17}$$

with $q = \sum_{i=1}^{p} q_i$. For the seniority-zero case, when $\Omega_i = 1/2 \ \forall \ i$ corresponding to $p$ Nilsson levels,

$$\eta(p,k) = \frac{p!}{(p-k)!k!}. \tag{18}$$

Hence, one may turn to find polynomial solutions of $y(x)$ satisfying (13)

In search for polynomial solutions of (13), we write

$$y(x) = \sum_{j=0}^{k} a_j x^j, \quad V(x) = \sum_{j=0}^{p-1} b_j x^j, \tag{19}$$

where $\{a_j\}$ and $\{b_j\}$ are the expansion coefficients to be determined. Substitution of (19) into equation (13) yields two matrix equations. Namely, the condition that the coefficients in front of $x^i$ $(i = 0, \ldots, k)$ must be zero yields a $(k+1) \times (k+1)$ matrix $\mathbf{F}$ with $\mathbf{Fv} = b_0\mathbf{v}$, where the eigenvector $\mathbf{v}$ of $\mathbf{F}$ is simply given by the expansion coefficients $\mathbf{v} = \{a_0, \ldots, a_k\}$. In addition, the condition that the coefficients in front of $x^i$ $(i = k+1, \ldots, p+k-1)$ must be zero yields another $(p-1) \times (k+1)$ upper-triangular matrix $\mathbf{P}$ with $\mathbf{Pv} = 0$, which provides a unique solution for $b_i$ $(i = 1, \ldots, p-1)$ in terms of $\{a_j\}$. Entries of the two matrices are all linear in the coefficients $\{b_1, b_2, \ldots, b_{p-1}\}$. Matrices $\mathbf{F}$ and $\mathbf{P}$ can be easily constructed, for which a simple MATHEMATICA code is available [35]. Once the polynomial is known, zeros of the single-variable $y(x)$ can easily be evaluated numerically.

According to the Stieltjes results [53], an electrostatic interpretation of the location of zeros of the polynomial $y(x)$ may be stated as follows [24,28,33]. Put $p$ negative fixed charges $\rho_t$ along a real line, and allow $k$ positive unit charges to move freely on the complex plane under such situation together with a uniform electric field with strength $1/(2G)$. Therefore, up to a constant, the total energy functional $U(x_1, \ldots, x_k)$ may be written as

$$U(x_1, \ldots, x_k) = \frac{1}{2G} \sum_{i}^{k} x_i - \sum_{it} \rho_t \ln|2\epsilon_{j_t} - x_i| - \sum_{i \neq i'} \ln|x_i - x_{i'}|. \tag{20}$$

In this case, there are $\eta(p,k)$ different configurations for the position of the $k$ positive charges $\{x_1^{(\xi)}, \ldots, x_k^{(\xi)}\}$ with $\xi = 1, 2, \ldots, \eta(p,k)$ corresponding to global minimums of the total energy.

Using the polynomial approach, one can evaluate ground-state quantities of the model and compared with experimental results, even when valence space is relatively larger. For example, the pairing gap of the ground states of Ni and Sm isotopes were calculated from the model [54], referred to as HS Pairing, which are compared with the corresponding experimental data. The results of $^{58-77}$Ni obtained by using the BCS approximation are also shown for comparison. In the calculation, the empirical like-particle pairing gap was estimated by the third derivative of binding energies,

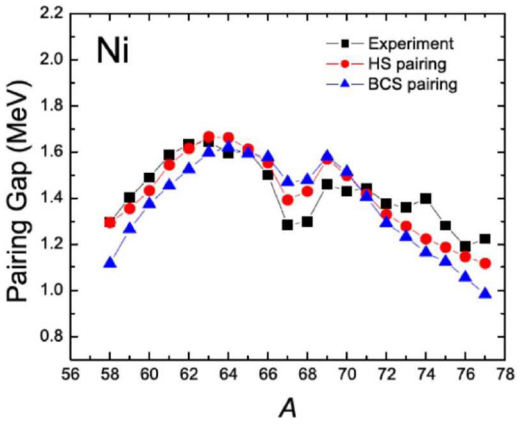


**Fig. 1.** Pairing gaps in MeV calculated by the HS pairing ●, the BCS approximation ▲, and compared to experimental data ■ of $^{58-77}$Ni with four $j$-orbits, $f_{5/2}$, $p_{1/2,\,3/2}$, $g_{9/2}$ and $G = 23/A$ MeV.

BE, with respect to the number of valence like-particles, which for neutrons is,

$$\Delta_{nn} \equiv \frac{1}{4}(BE(Z, N-2) - 3BE(Z, N-1) + 3BE(Z, N) - BE(Z, N+1)). \quad (21)$$

It is found that the model with paring strength $G = 23/A$ MeV yields a close reproduction of experimental results of $^{58-77}$Ni as shown in Figure 1.

## 2.2 Mean-field plus special separable pairing

The Hamiltonian of a mean-field plus separable pairing model (SP) may be written as [55]

$$\hat{H} = \sum_{t=1}^{p} \epsilon_{j_t} \hat{N}_{j_t} + \hat{H}_{\rm P} = \sum_{t=1}^{p} \epsilon_{j_t} \hat{N}_{j_t} - G \sum_{1 \le t,t' \le p} c_{j_t} c_{j_{t'}} S^{+}_{j_t} S^{-}_{j_{t'}}. \quad (22)$$

It is known from [55] that the exact solution of (22) becomes very complicated and tedious for $p \geq 3$. Nevertheless, there is a special case like the standard pairing that can be solved exactly, of which the parameters $\{c_{j_t}\}$ satisfy [56–58]

$$(c_{j_t})^2 = g_1 \epsilon_{j_t} + g_2 \ \forall \ \ t, \quad (23)$$

where $g_1$ and $g_2$ are parameters to be determined. It is obvious that the model becomes the standard pairing case when $g_2$ is a constant and $g_1 = 0$.

Similar to the standard pairing, $k$-pair eigenstate of (22) in this case can also be expressed in the form of (9), but the paring operator $S^{+}(x)$ should be of the following form [56]:

$$S^{+}(x) = \sum_{t=1}^{p} \frac{1}{2\epsilon_{j_t} - x} c_{j_t} S^{+}_{j_t}. \quad (24)$$

According to the commutation relations given in (4), we have

$$\left[\sum_t \epsilon_{j_t}\hat{N}_{j_t},\ S^+(x)\right] = \sum_t \frac{2\epsilon_{j_t}}{2\epsilon_{j_t}-x} c_{j_t} S^+_{j_t} = \sum_t c_{j_t} S^+_{j_t} + xS^+(x), \tag{25}$$

$$[\hat{H}_{\rm P},\ S^+(x)] = G\sum_{t'} c_{j_{t'}} S^+_{j_{t'}} \sum_t \frac{2S^0_{j_t}(c_{j_t})^2}{2\epsilon_{j_t}-x} = G\sum_{j_{t'}} c_{j_{t'}} S^+_{j_{t'}} \Lambda_1(x), \tag{26}$$

where $\Lambda_1(x) = \sum_t \frac{2S^0_{j_t}(c_{j_t})^2}{2\epsilon_{j_t}-x}$, and

$$\begin{aligned} S^+(x,y) &= [[\hat{H}_{\rm P},\ S^+(x)],\ S^+(y)] \\ &= G\sum_{t'} c_{j_{t'}} S^+_{j_{t'}} \left(\frac{g_1}{x-y}(xS^+(x)-yS^+(y)) + \frac{2g_2}{x-y}(S^+(x)-S^+(y))\right). \end{aligned} \tag{27}$$

One can verify that the eigen-equation $\hat{H}||\xi;k;\nu\eta JM\rangle = E^{(\xi)}_k|\xi;k;\nu\eta JM\rangle$ is fulfilled when and only when

$$\sum_{t=1}^{p} \frac{(g_1\epsilon_{j_t}+g_2)(\Omega_{j_t}-\nu_{j_t})}{2\epsilon_{j_t}-x^{(\xi)}_i} + \sum_{l\neq i} \frac{g_1 x^{(\xi)}_l + 2g_2}{x^{(\xi)}_i - x^{(\xi)}_l} = 1/G \quad \text{for} \quad i=1,2,\ldots k, \tag{28}$$

with the corresponding eigen-energy still given by (12).

According to Heine–Stieltjes correspondence, for nonzero $G$, zeros $\{x^{(\xi)}_i\}$ of the extended Heine–Stieltjes polynomials $y_k(x)$ of degree $k$ are roots of equation (28), where $y_k(x)$ should still satisfy the second-order Fuchsian equation (13). For this case, $A(x) = \frac{1}{2}(g_1x+2g_2)\prod_{t=1}^{p}(2\epsilon_{j_t}-x)$ is a polynomial of degree $p+1$, the polynomial $B(x,k)$ of degree $p-1$ is given as

$$B(x,k)/A(x) = \frac{2}{g_1x+2g_2}\sum_{t=1}^{p}\frac{(g_1\epsilon_{j_t}+g_2)(\Omega_{j_t}-\nu_{j_t})}{2\epsilon_{j_t}-x} - \frac{2(k-1)Gg_1+2}{(g_1x+2g_2)G}, \tag{29}$$

where the identity

$$\sum_{1\le l(\neq i)\le k} \frac{x^{(\xi)}_l}{x^{(\xi)}_i - x^{(\xi)}_l} = x^{(\xi)}_i \sum_{1\le l(\neq i)\le k} \frac{1}{x^{(\xi)}_i - x^{(\xi)}_l} - (k-1) \tag{30}$$

is used.

### 2.3 Mean-field plus special non-separable pairing

It is shown in a recent work [59] that there is an extension of the special separable pairing interaction with the Hamiltonian given by

$$\hat{H} = \sum_t^p \epsilon_t \hat{N}_{j_t} + \hat{H}_{\rm P} = \sum_t^p \epsilon_t \hat{N}_{j_t} + \sum_{1\le t,t'\le p} g_{t,t'} S^+_{j_t} S^-_{j_{t'}} \tag{31}$$

with

$$g_{tt'} = \sum_{\mu,\nu} G_{\mu,\nu} (c_t)^{\mu} (c_{t'})^{\nu}, \tag{32}$$

where $\mu$, $\nu$ only run over $+1$ and $-1$. Thus, the pairing interaction $\hat{H}_{\rm P}$ can be expressed as

$$\hat{H}_{\rm P} = G_{+,+}\, S_1^+ S_1^- + G_{+,-}\, S_1^+ S_{-1}^- + G_{-,+}\, S_{-1}^+ S_1^- + G_{-,-}\, S_{-1}^+ S_{-1}^-, \tag{33}$$

where $S_\mu^\pm = \sum_{t=1}^{p} (c_t)^\mu\, S_{j_t}^\pm$ for $\mu = \pm 1$. As adopted in the separable pairing, let the $k$-pair eigenvectors of (31) can be written in the form of (9) with the paring operator $S^+(x)$ the same as that shown in (24). For $p = 3$, $S^+(x)$ is a trinomial in $S_{j_t}^+$ with 3 independent terms. Hence, we have

$$\left[\sum_t \epsilon_t\, \hat{N}_{j_t},\ S^+(x)\right] = \sum_t \frac{2\epsilon_t}{c_t^2 - x}\, c_t\, S_{j_t}^+ = \alpha(x)\, S^+(x) + \beta(x)\, S_1^+ + \gamma(x)\, S_{-1}^+, \tag{34}$$

where $\alpha(x)$, $\beta(x)$, and $\gamma(x)$ are independent functions of $x$ with

$$\begin{aligned}
\alpha(x) &= \frac{2\,(c_1^2(c_2^2 - c_3^2)(x - c_2^2)(x - c_3^2)\,\epsilon_1 - c_2^2(c_1^2 - c_3^2)(x - c_1^2)(x - c_3^2)\,\epsilon_2 + c_3^2(c_1^2 - c_2^2)(x - c_1^2)(x - c_2^2)\,\epsilon_3)}{(c_1^2 - c_2^2)(c_1^2 - c_3^2)(c_2^2 - c_3^2)\,x}, \\
\beta(x) &= \beta = \frac{2\,c_1^2 c_2^2(\epsilon_1 - \epsilon_2) + 2\,c_1^2 c_3^2(\epsilon_3 - \epsilon_1) + 2\,c_2^2 c_3^2(\epsilon_2 - \epsilon_3)}{(c_1^2 - c_2^2)(c_1^2 - c_3^2)(c_2^2 - c_3^2)}, \\
\gamma(x) &= \gamma/x = \frac{2\,c_1^2 c_2^2 c_3^2\,\left(c_1^2(\epsilon_2 - \epsilon_3) + c_3^2(\epsilon_1 - \epsilon_2) + c_2^2(\epsilon_3 - \epsilon_1)\right)}{(c_1^2 - c_2^2)(c_1^2 - c_3^2)(c_2^2 - c_3^2)\,x}
\end{aligned} \tag{35}$$

for $p = 3$, where $c_1 \neq c_2 \neq c_3$ is assumed. More generally, the parameters $\{\epsilon_t\}$ and $\{c_t\}$ $(t = 1,\ 2, \ldots, p)$ must satisfy the constraints

$$\epsilon_t = \frac{1}{2}\left(u_0 + u_2 (c_t)^2 + u_{-2} (c_t)^{-2}\right) \tag{36}$$

for $t = 1, 2, \ldots, p$, where $u_0$, $u_2$, and $u_{-2}$ are another three free parameters with

$$\alpha(x) = u_0 + u_2\, x - \frac{u_{-2}}{x}, \quad \beta = u_2, \quad \gamma(x) = -\frac{u_{-2}}{x} \tag{37}$$

for $p \geq 3$.

Using equations (4), (24), and (34), one can directly check that

$$\sum_t \epsilon_t \hat{N}_{j_t}|\xi;k;\nu\eta JM\rangle = \sum_i^k \left(\beta\, S_1^+ + \gamma(x_i^{(\xi)})\, S_{-1}^+\right) \prod_{\rho\,(\neq i)}^k S^+(x_\rho^{(\xi)})|\nu\eta JM\rangle + \left(\sum_i^k \alpha(x_i^{(\xi)}) + \sum_{t=1}^p \epsilon_t\nu_t\right) \prod_\rho^k S^+(x_\rho^{(\xi)})|\nu\eta JM\rangle \quad (38)$$

and

$$\begin{aligned}\hat{H}_{\rm P}|\xi;k;\nu\eta JM\rangle = &-\sum_i^k \Big(S_1^+(\,G_{+,+}\,\Lambda_1(x_i^{(\xi)}) + G_{+,-}\,\Lambda_0(x_i^{(\xi)})\,) \\ &+ S_{-1}^+(G_{-,+}\,\Lambda_1(x_i^{(\xi)}) + G_{-,-}\,\Lambda_0(x_i^{(\xi)})\,)\Big) \prod_{\rho(\neq i)}^k S^+(x_\rho^{(\xi)})|\nu\eta JM\rangle \\ &-S_1^+ \sum_i^k \sum_{i'\,(\neq i)}^k (G_{+,+}\frac{2x_{i'}^{(\xi)}}{x_{i'}^{(\xi)} - x_i^{(\xi)}} \\ &+G_{+,-}\frac{2}{x_{i'}^{(\xi)} - x_i^{(\xi)}}) \prod_{\rho\,(\neq i)}^k S^+(x_\rho^{(\xi)})|\nu\eta JM\rangle \\ &-S_{-1}^+ \sum_i^k \sum_{i'\,(\neq i)}^k (G_{-,+}\frac{2x_{i'}^{(\xi)}}{x_{i'}^{(\xi)} - x_i^{(\xi)}} \\ &+G_{-,-}\frac{2}{x_{i'}^{(\xi)} - x_i^{(\xi)}}) \prod_{\rho\,(\neq i)}^k S^+(x_\rho^{(\xi)})|\nu\eta JM\rangle, \end{aligned} \quad (39)$$

where

$$\Lambda_\mu(x) = -\sum_t \frac{(\Omega_t - \nu_t)(c_t^2)^\mu}{c_t^2 - x}. \quad (40)$$

Similar to the special separable pairing, the eigenvalue $E_k^{(\xi)}$ is now given by

$$E_k^{(\xi)} = \sum_{t=1}^p \epsilon_t\nu_t + \sum_{i=1}^k \alpha(x_i^{(\xi)}), \quad (41)$$

with $2k$ equations in determining the $k$ variables $\{x_i^{(\xi)}\}$:

$$\beta - G_{+,+}\,F(x_i^{(\xi)}) - G_{+,-}\,V(x_i^{(\xi)}) = 0 \quad \text{for } i = 1, 2, \ldots, k, \quad (42)$$

$$\frac{\gamma}{x_i^{(\xi)}} - G_{-,+}\,F(x_i^{(\xi)}) - G_{-,-}\,V(x_i^{(\xi)}) = 0 \quad \text{for } i = 1, 2, \ldots, k, \quad (43)$$

where

$$F(x_i^{(\xi)}) = \Lambda_1(x_i^{(\xi)}) + \sum_{i'\,(\neq i)}^{k} \frac{2x_{i'}^{(\xi)}}{x_{i'}^{(\xi)} - x_i^{(\xi)}}, \quad V(x_i^{(\xi)}) = \Lambda_0(x_i^{(\xi)}) + \sum_{i'\,(\neq i)}^{k} \frac{2}{x_{i'}^{(\xi)} - x_i^{(\xi)}}. \tag{44}$$

Since $\beta$ and $\gamma$ are all nonzero in general, the Hamiltonian (31) with $G_{+,+} \neq 0$, $G_{+,-} \neq 0$, $G_{-,+} \neq 0$, and $G_{-,-} \neq 0$ cannot be diagonalized by using the ansatz (9) with the paring operator $S^+(x)$ the same as that shown in (24) because (42) and (43) cannot be simultaneously satisfied in this case. Nevertheless, there are two special cases for nonzero $\{c_t\}$ $(t = 1, 2, \ldots, p)$ that can be solved exactly. One is $\gamma = 0$ case corresponding to $u_{-2} = 0$, while another is $\beta = 0$ case corresponding to $u_2 = 0$. The former case with $G_{+,+} \neq 0$, $G_{+,-} = G_{-,+} = G_{-,-} = 0$ is just the special separable pairing (SSP) case discussed in [56–58], while the latter case with $G_{-,-} \neq 0$, $G_{+,-} = G_{-,+} = G_{+,+} = 0$ is equivalent to the former one with the replacements: $c_t \to c_t^{-1}$ for $t = 1, 2, \ldots, p$. When

$$\frac{\beta - G_{+,+}\,(2(k-1) - \Omega)}{G_{+,+}} = \frac{\gamma}{G_{-,-}} \tag{45}$$

is satisfied, two sets of equations (42) and (43) coalesce into $k$ equations in determining the $k$ variables

$$\frac{\gamma}{G_{-,-}} - x_i^{(\xi)}\, V(x_i^{(\xi)}) = 0 \quad \text{for } i = 1, 2, \ldots, k. \tag{46}$$

For this case, the pairing interaction matrix elements (32) can be expressed in terms of $p + 2$ parameters $\{c_1, c_2, \ldots, c_p\}$, $G_{+,+}$, and $G_{-,-}$ as

$$g_{tt'} = G_{+,+}\, c_t\, c_{t'} + \frac{G_{-,-}}{c_t\, c_{t'}} \tag{47}$$

with the constraints (36) and (45), which are obviously non-separable in general.

To demonstrate the solution of both the Special Separable Pairing (SSP) and the Special Non-Separable Pairing (SNSP), we consider the $ds$-shell with 3 orbitals $0d_{5/2}$, $1s_{1/2}$, and $0d_{3/2}$, of which the single-particle energies are provided in [60]. The effective pairing interaction matrix elements $\{G_{t,t'}\}$ in the $\{S_{j_t}^+\}$ basis with $\hat{H}_{\rm Pairing} = \sum_{jj'} G_{t,t'} S_{j_t}^+ S_{j_{t'}}^-$ for this case are obtained from the $J = 0$ and $T = 1$ two-body matrix elements of the SDPF–NR interaction [60], where $j_1 = 1/2$, $j_2 = 5/2$, and $j_3 = 3/2$ are assigned, and the mass scaling factor $(A/18)^{1/3}$ of the two-body matrix elements is not included. The separable pairing interaction parameters $\{c_j\}$ may be determined from the two-particle ground state of the mean-field plus the $\hat{H}_{\rm Pairing}$, of which the expansion coefficients of the two-particle ground state in terms of $\{S_j^+\}$ may be taken to be the corresponding separable pairing interaction parameter $\{c_j\}$ of the spherical mean-field plus the separable pairing model (SP) [55]. The overall pairing strength in the SP was adjusted to reproduce the same two-particle ground state energy, which is thus fixed though it also varies with $k$. Then, a linear fit of $\{c_j^2\}$ by the single-particle energies with $1 \geq c_j^2 = g_1\epsilon_j + g_2 \geq 0$ is performed according to the constraint shown in (23). The best linear fit in the SSP yields $c_j^2 = 0.1524 - 0.067\epsilon_j$ for the $ds$-shell [56]. Since the overall pairing strength varies with the number of pairs $k$, the overall pairing interaction strength in the SSP was then adjusted to reproduce the same ground state energy of the SP for a given $k$. In the SNSP, because $\{g_{t,t'}\}$ obtained

from the SNSP (47) are independent of one of nonzero $c_i$ $(i = 1, 2, 3)$ due to (45), only $c_1$, $c_2$, and $G_{+,+}$ were taken as fitting parameters, while $G_{-,-}$ is determined according to (45). The fitting results of $\{g_{t,t'}\}$ are independent of nonzero $c_3$ in this case. Hence, $c_3 = 1$ is taken in the calculation. Thus, one can use 3 of the 6 pairing interaction matrix elements $G_{t,t'}$ to get $c_1$, $c_2$, and $G_{+,+}$ shown in Table 1. The pairing excitation energies $E_k^{(\xi)}$ of the seniority-zero case up to the half-filling case obtained from the SP, the SSP, the SNSP are shown in Table 2, in which the results of the SPM with $g_{tt'} = G$ used in (3) are also shown for comparison. Since the SP results are closer to those obtained from the Hamiltonian with the experimentally determined pairing interaction matrix elements $G_{t,t'}$ [60], the $\chi^2$ deviation defined by

$$\chi^2 = \frac{1}{s}\sum_{\xi=1}^{s}\left(E_{\rm SP}^{(\xi)} - E^{(\xi)}\right)^2 \tag{48}$$

is adopted, where $E_{\rm SP}^{(\xi)}$ are pairing excitation energies of the SP, $E^{(\xi)}$ are those of the SNSP, the SSP, and the SMP, respectively, and $s$ is the total number of pairing excitation states for given $k$, of which the corresponding value for each model is also shown in the last row of Table 2. It can be observed from Table 2 that the SNSP and the SSP results are quite similar and closer to the corresponding SP values, while there are larger deviations of the SPM results from those of the SP. Therefore, both the SNSP and the SSP are more accurate in pairing excitation energies. The situation in the $fp$-shell is quite the same [56,59].

### 2.4 Non-separable pairing for two-orbit case

Besides the SSP and the SNSP, the Bethe–Gaudin–Richardson method can also be applied to get the exact solution of the general orbit-dependent non-separable pairing with two non-degenerate $j$-orbits [61]. The Hamiltonian of a spherical mean-field plus orbit-dependent non-separable pairing model (NSPM) with two non-degenerate $j$-orbits can be written as [61]

$$\hat{H} = \sum_{t}^{p}\epsilon_t\,\hat{N}_{j_t} + \hat{H}_{\rm P} = \sum_{t}^{p}\epsilon_t\,\hat{N}_{j_t} - \sum_{1\le t,t'\le p} g_{t,t'}\,S_{j_t}^{+}S_{j_{t'}}^{-}, \tag{49}$$

where $p = 2$ is the total number of orbits considered above a closed or sub-closed shell. As adopted in the Richardson–Gaudin approach for the SPM, let

$$S^{+}(x) = \sum_{t=1}^{2}\frac{1}{2\epsilon_t - x}S_{j_t}^{+}. \tag{50}$$

According to the commutation relations of the generators of the two copies of the SU(2) algebra, we have

$$\left[\sum_{t}\epsilon_t\hat{N}_{j_t},\ S^{+}(x)\right] = \sum_{t}\frac{2\epsilon_t}{2\epsilon_t - x}S_{j_t}^{+} = S^{+} + x\,S^{+}(x), \tag{51}$$

**Table 1.** The single-particle energies $\epsilon_j$ (in MeV), the pairing interaction matrix elements $G_{t,t'}$ (in MeV) in the $\{S_j^+\}$ basis of the $ds$-shell [60], and the parameters of the SNSP, where $g_{t,t'}$ (in MeV) are the fitting results [59] of the SNSP obtained by using the parameters $c_1$, $c_2$, and $G_{+,+}$ for given $k$ with $G_{-,-} = G_{+,+}^*$ provided in the corresponding row of the table, and $\mathrm{i} = \sqrt{-1}$.

| | |
|---|---|
| The $ds$-shell [60] | $\epsilon_1 = \epsilon_{1/2} = -2.92 \quad \epsilon_2 = \epsilon_{5/2} = -3.70 \quad \epsilon_3 = \epsilon_{3/2} = 1.90$<br>$G_{1,1} = -1.075 \quad G_{2,2} = -0.728 \quad G_{3,3} = -0.410 \quad G_{1,2} = 0.121 \quad G_{2,3} = -0.355 \quad G_{1,3} = 0.000$ |
| $k = 1$ | $g_{1,1} = -0.765 \quad g_{2,2} = -0.580 \quad g_{3,3} = -0.340 \quad g_{1,2} = 0.677 \quad g_{2,3} = -1.038 \quad g_{1,3} = 1.015$<br>$c_1 = -0.544 + 0.839\,\mathrm{i} \quad c_2 = -0.443 - 0.896\,\mathrm{i} \quad G_{+,+} = (-0.17 - 0.495\,\mathrm{i})$ MeV |
| $k = 2$ | $g_{1,1} = -0.710 \quad g_{2,2} = -0.580 \quad g_{3,3} = -0.340 \quad g_{1,2} = 0.649 \quad g_{2,3} = -0.835 \quad g_{1,3} = 0.812$<br>$c_1 = -0.646 + 0.763\,\mathrm{i} \quad c_2 = -0.551 - 0.835\,\mathrm{i} \quad G_{+,+} = (-0.17 - 0.388\,\mathrm{i})$ MeV |
| $k = 3$ | $g_{1,1} = -0.573 \quad g_{2,2} = -0.580 \quad g_{3,3} = -0.340 \quad g_{1,2} = 0.577 \quad g_{2,3} = -0.508 \quad g_{1,3} = 0.493$<br>$c_1 = -0.925 + 0.379\,\mathrm{i} \quad c_2 = 0.905 - 0.426\,\mathrm{i} \quad G_{+,+} = (-0.17 - 0.236\,\mathrm{i})$ MeV |

**Table 2.** Comparison of pairing excitation energies $E_k^{(\xi)}$(in MeV) of the seniority-zero case obtained from the SNSP with those of the SP [55] for a given number of pairs $k$ up to the half-filling, where $g_{t,t}$ in the SNSP are adjusted to $E_{k=1}^{(\xi)}$ of the SP indicated by $^*$, while $g_{1,1}$ for given $k$ in the SNSP is then adjusted to ground-state energy $E_k^{(\xi=1)}$ of the SP indicated by $^*$, the overall strength $G$ in the SPM and the pairing parameters in the SSP are adjusted to produce the ground-state energy $E_{k=1}^{(\xi=1)}$ of the SP indicated by $^*$.

| | $k=1$ | | | | $k=2$ | | | | $k=3$ | | | |
|---|---|---|---|---|---|---|---|---|---|---|---|---|
| | SP | SNSP | SSP | SPM | SP | SNSP | SSP | SPM | SP | SNSP | SSP | SPM |
| $\xi=1$ | $-10.22^*$ | $-10.22^*$ | $-10.22$ | $-10.22^*$ | $-18.56$ | $-18.56^*$ | $-18.82$ | $-18.89$ | $-25.03$ | $-25.03^*$ | $-25.81$ | $-25.97$ |
| $\xi=2$ | $-5.84$ | $-6.16$ | $-6.09$ | $-6.12$ | $-16.05$ | $-15.18$ | $-15.44$ | $-15.39$ | $-24.38$ | $-22.83$ | $-23.26$ | $-23.21$ |
| $\xi=3$ | 3.79 | 3.76 | 3.72 | 2.72 | $-6.42$ | $-6.16$ | $-6.48$ | $-7.20$ | $-14.76$ | $-14.56$ | $-15.08$ | $-15.86$ |
| $\xi=4$ | | | | | $-2.05$ | $-2.78$ | $-2.37$ | $-3.53$ | $-12.25$ | $-11.81$ | $-11.72$ | $-12.76$ |
| $\xi=5$ | | | | | 7.59 | 7.33 | 7.52 | 6.49 | $-2.62$ | $-2.30$ | $-2.65$ | $-3.25$ |
| $\xi=6$ | | | | | | | | | 1.75 | 0.92 | 1.42 | 0.26 |
| $\chi^2$ | | 0.034 | 0.022 | 0.408 | | 0.285 | 0.110 | 0.911 | | 0.571 | 0.393 | 1.053 |

where $S^+ = \sum_t S^+_{j_t}$, and

$$[\hat{H}_{\rm P},\ S^+(x)] = \sum_{t',t} g_{t',t} S^+_{j_{t'}} \frac{2S^0_{j_t}}{2\epsilon_t - x}, \tag{52}$$

$$[[\hat{H}_{\rm P},\ S^+(x)],\ S^+(y)] = 2\sum_{t',t} g_{t',t} \frac{1}{(2\epsilon_t - x)(2\epsilon_t - y)} S^+_{j_{t'}} S^+_{j_t}. \tag{53}$$

The $k$-pair eigenvectors of (49) can be still written as the Richardson-Gaudin form (9). Since the Hamiltonian (49) only contains one- and two-body interaction terms, the $q$-time commutators $[\ldots[\hat{H}, S^+(x^{(\zeta)}_{\rho_1})], \ldots, S^+(x^{(\zeta)}_{\rho_{q-1}})], S^+(x^{(\zeta)}_{\rho_q})]$ vanish when $q \geq 3$. Namely, one only needs to calculate single and double commutators of $\hat{H}$ with the operators $S^+(x^{(\zeta)}_{\rho})$. The commutator applied to the vacuum state $|\nu\eta JM\rangle$ gives

$$\begin{aligned}[\hat{H}_{\rm P},\ S^+(x)]|\nu\eta JM\rangle &= \sum_{t',t} g_{t',t}\, S^+_{j_{t'}} \frac{2S^0_{j_t}}{2\epsilon_t - x}|\nu\eta JM\rangle \\ &= (\alpha(x)\, S^+ + \beta(x)\, S^+(x))|\nu\eta JM\rangle. \end{aligned} \tag{54}$$

After solving the above binomial equations of the local operators $S^+_{j_1}$ and $S^+_{j_2}$, one obtains

$$\begin{aligned}\alpha(x) &= -\frac{(x-2\epsilon_2)\left((x-2\epsilon_1)g_{1,1} - (x-2\epsilon_2)g_{1,2}\right)(\Omega_1 - \nu_1) + (x-2\epsilon_1)\left((x-2\epsilon_1)g_{1,2} - (x-2\epsilon_2)g_{2,2}\right)(\Omega_2 - \nu_2)}{2(x-2\epsilon_1)(x-2\epsilon_2)(\epsilon_1 - \epsilon_2)}, \\ \beta(x) &= -\frac{(x-2\epsilon_2)(g_{1,1} - g_{1,2})(\Omega_1 - \nu_1) + (x-2\epsilon_1)(g_{1,2} - g_{2,2})(\Omega_2 - \nu_2)}{2(\epsilon_1 - \epsilon_2)}, \end{aligned} \tag{55}$$

where the condition $g_{2,1} = g_{1,2}$ is used. Similarly, the double commutator can be expressed as

$$\begin{aligned}[[\hat{H}_{\rm P},\ S^+(x)],\ S^+(y)] &= 2\sum_{t',t} g_{t',t} \frac{1}{(2\epsilon_t - x)(2\epsilon_t - y)} S^+_{j_{t'}} S^+_{j_t} \\ &= a(x,y)\, S^+ S^+(x) + b(x,y)\, S^+ S^+(y) + c(x,y)\, S^+(x) S^+(y), \end{aligned} \tag{56}$$

which expressed in terms of $S^+$, $S^+(x)$, and $S^+(y)$ is only possible for two $j$-orbit case. For a system with $p$ $j$-orbits, $p(p+1)/2$ terms are needed on the right-hand-side of (56). For example, six terms on the right-hand-side of (56) are needed for the three $j$-orbit case.

After comparing the coefficients of $S^+_{j_t} S^+_{j_{t'}}$ with the same $t$ and $t'$ on both sides of (56), one gets

$$\begin{aligned} a(x,y) &= \frac{1}{2(x-y)(\epsilon_1 - \epsilon_2)^2} F(x,y), \quad b(x,y) = a(y,x), \\ c(x,y) &= \frac{1}{2(\epsilon_1 - \epsilon_2)^2}\left((x+y)(2\epsilon_2(g_{1,2} - g_{1,1}) + 2\epsilon_1(g_{1,2} - g_{2,2})) \right. \\ &\quad \left. + x\, y\,(g_{1,1} + g_{2,2} - 2g_{1,2}) + 4\epsilon_2^2(g_{1,1} - g_{1,2}) + 4\epsilon_1^2(g_{2,2} - g_{1,2})\right), \end{aligned} \tag{57}$$

which is obviously symmetric in $x$ and $y$, where

$$\begin{aligned} F(x,y) = & \, x\,(2\epsilon_1(g_{1,1}-g_{1,2})+2\epsilon_2(g_{2,2}-g_{1,2})) \\ & + y\,(2\epsilon_2(g_{1,1}-g_{1,2})+2\epsilon_1(g_{2,2}-g_{1,2})) \\ & + x\,y\,(2g_{1,2}-g_{1,1}-g_{2,2})+4g_{1,2}(\epsilon_1^2+\epsilon_2^2)-4\epsilon_1\epsilon_2(g_{1,1}+g_{2,2}). \end{aligned} \quad (58)$$

It can be verified that the eigen-equation $\hat{H}|\xi;k;\nu\eta JM\rangle = E_k^{(\xi)}|\xi;k;\nu\eta JM\rangle$ is fulfilled if and only if

$$1+\alpha\left(x_i^{(\xi)}\right)+\sum_{i'\,(\neq i)}^{k} a(x_{i'}^{(\xi)},x_i^{(\xi)}) = 0 \quad \text{for} \quad i=1,2,\ldots k, \quad (59)$$

with the corresponding eigen-energy

$$\begin{aligned} E_k^{(\xi)} = & \sum_{t=1}^{p}\epsilon_t\nu_t+\sum_{i=1}^{k}\left(x_i^{(\xi)}+\beta(x_i^{(\xi)})+\sum_{i'=i+1}^{k} c(x_i^{(\xi)},x_{i'}^{(\xi)})\right) = \sum_{t=1}^{p}\epsilon_t\nu_t \\ & + \left(\frac{(g_{1,1}-g_{1,2})(\Omega_1-\nu_1)\epsilon_2}{\epsilon_1-\epsilon_2}+\frac{(g_{1,2}-g_{2,2})(\Omega_2-\nu_2)\epsilon_1}{\epsilon_1-\epsilon_2}+\frac{\epsilon_1^2(g_{2,2}-g_{1,2})+\epsilon_2^2(g_{1,1}-g_{1,2})}{(\epsilon_1-\epsilon_2)^2}(k-1)\right)k \\ & + \left(1-\frac{(g_{1,1}-g_{1,2})(\Omega_1-\nu_1)}{2\epsilon_1-2\epsilon_2}-\frac{(g_{1,2}-g_{2,2})(\Omega_2-\nu_2)}{2\epsilon_1-2\epsilon_2}+\frac{\epsilon_2(g_{1,2}-g_{1,1})+\epsilon_1(g_{1,2}-g_{2,2})}{(\epsilon_1-\epsilon_2)^2}(k-1)\right) \\ & \times \sum_{i=1}^{k} x_i^{(\xi)}+\frac{g_{1,1}+g_{2,2}-2g_{1,2}}{4(\epsilon_1-\epsilon_2)^2}\left(\left(\sum_{i=1}^{k}x_i^{(\xi)}\right)^2-\sum_{i=1}^{k}\left(x_i^{(\xi)}\right)^2\right). \end{aligned} \quad (60)$$

Similar to the SPM, the solutions of (59) are zeros of $y(x)$ satisfying

$$A(x)\,y_k''(x)+B(x,k)\,y_k'(x)-V(x,k)\,y_k(x)=0. \quad (61)$$

Here,

$$A(x)=\frac{1}{2}(x^2F_{12}+x\,(F_1+F_2)+F_0)\prod_{t=1}^{2}(2\epsilon_t-x) \quad (62)$$

is a polynomial of degree 4, in which

$$\begin{aligned} F_1 = \tfrac{\epsilon_1(g_{1,1}-g_{1,2})+\epsilon_2(g_{2,2}-g_{1,2})}{(\epsilon_1-\epsilon_2)^2},\ F_2 = \tfrac{\epsilon_2(g_{1,1}-g_{1,2})+\epsilon_1(g_{2,2}-g_{1,2})}{(\epsilon_1-\epsilon_2)^2}, \\ F_{12} = \tfrac{2g_{1,2}-g_{1,1}-g_{2,2}}{2(\epsilon_1-\epsilon_2)^2},\ F_0 = \tfrac{2g_{1,2}(\epsilon_1^2+\epsilon_2^2)-2\epsilon_1\epsilon_2(g_{1,1}+g_{2,2})}{(\epsilon_1-\epsilon_2)^2}, \end{aligned} \quad (63)$$

the polynomial $B(x,k)$ of degree 3 is given as

$$\begin{aligned} & B(x,k)/A(x) \\ & = \frac{2}{x^2F_{12}+x\,(F_1+F_2)+F_0}\left(\sum_{t=1}^{2}\frac{\alpha_t^{(1)}+\alpha_t^{(2)}\,x}{2\epsilon_t-x}-(F_1+F_{12}\,x)\,(k-1)-1\right), \end{aligned} \quad (64)$$

where

$$\begin{aligned} \alpha_1^{(1)} = \tfrac{(\epsilon_1 g_{1,1}-\epsilon_2 g_{1,2})(\Omega_1-\nu_1)}{\epsilon_1-\epsilon_2},\ \alpha_1^{(2)} = \tfrac{(g_{1,2}-g_{1,1})(\Omega_1-\nu_1)}{2\epsilon_1-2\epsilon_2}, \\ \alpha_2^{(1)} = \tfrac{(\epsilon_1 g_{1,2}-\epsilon_2 g_{2,2})(\Omega_2-\nu_2)}{\epsilon_1-\epsilon_2},\ \alpha_2^{(2)} = \tfrac{(g_{2,2}-g_{1,2})(\Omega_2-\nu_2)}{2\epsilon_1-2\epsilon_2}. \end{aligned} \quad (65)$$

**Table 3.** Excited level energies $E^{(\xi)}$ (in MeV) of the NSPM and the overlap-square $\eta(\xi) = |\langle\xi|\xi\rangle_{\rm SP}|^2$ of the pairing excited states with the corresponding ones of the SPM for $k = 5$ pairs over $j_1 = 19/2$ and $j_2 = 21/2$ orbits with single-particle energies $\epsilon_1 = 1$ MeV, $\epsilon_2 = 2$ MeV, and $g_{1,1} = g_{2,2} = 1$ MeV, where $g_{1,2} = \mathsf{g}$, and $\delta g = \mathsf{g} - g_{1,1}$ (in MeV). The overall pairing strength in the SPM is adjusted to reproduce the same ground-state energy of the NSPM for each case, with which the corresponding overlap $\eta(\xi)$ is obtained.

| | | $0_1^+$ | $0_2^+$ | $0_3^+$ | $0_4^+$ | $0_5^+$ | $0_6^+$ |
|---|---|---|---|---|---|---|---|
| $\delta g = -0.50$ | $E^{(\zeta)}$ | −48.95 | −36.66 | −26.23 | −17.30 | −9.90 | −4.96 |
| | $\eta(\zeta)$ | 99.600% | 98.989% | 97.968% | 96.600% | 95.370% | 94.548% |
| $\delta g = -0.25$ | $E^{(\zeta)}$ | −59.35 | −42.61 | −28.02 | −15.10 | −3.86 | 4.93 |
| | $\eta(\zeta)$ | 99.949% | 99.870% | 99.756% | 99.653% | 99.714% | 99.714% |
| $\delta g = 0.25$ | $E^{(\zeta)}$ | −80.28 | −54.81 | −31.93 | −10.96 | 8.34 | 25.66 |
| | $\eta(\zeta)$ | 99.977% | 99.946% | 99.905% | 99.883% | 99.9287% | 99.929% |
| $\delta g = 0.50$ | $E^{(\zeta)}$ | −90.78 | −60.98 | −33.94 | −8.91 | 14.49 | 36.12 |
| | $\eta(\zeta)$ | 99.934% | 99.842% | 99.728% | 99.674% | 99.806% | 99.818% |

To demonstrate the use of the solution, the validity of the SPM was analyzed. We consider 5 pairs in the NSPM with $\epsilon_1 = 1$ MeV and $\epsilon_2 = 2$ MeV, $j_1 = 19/2$ and $j_2 = 21/2$, with which each orbit can accommodate 5 pairs. The on-site pairing interaction parameters $g_{1,1} = g_{2,2} = 1$ MeV are fixed. We calculated the pair excitation energies of the NSPM for serval values of $g_{1,2} = \mathsf{g}$, which are presented in Table 3. Then, the overall pairing interaction strength of the SPM is adjusted according to the ground-state energy of the NSPM for each case. Though pairing excitation energies of the SPM are about 2 MeV different from the corresponding ones of the NSPM, as shown in Table 3, the overlap-square of the NSPM with the corresponding one of the SPM, $\eta(\xi) = |\langle\xi|\xi\rangle_{\rm SPM}|^2$, is always greater than 94% calculated in this way, where $|\xi\rangle \equiv |\xi, k = 5; 0\,0\rangle$ is obtained according to (16) for each case, while $|\xi\rangle_{\rm SPM}$ is the corresponding eigen-state of the SPM. The results of the overlaps show that the SPM seem a good approximation to the NSPM. In fact, with the increasing of the pairing interaction strength g of nucleon pairs from different orbits, the system undergoes a phase crossover from localized normal phase mainly determined by the pure mean-field and the on-site pairing interaction strengths $g_{t,t}$ $(t = 1, 2)$ among nucleon pairs within the same orbits to the delocalized superconducting phase, for which there are a few effective order parameters. Here we calculate the occupation probability of nucleon pairs in the $j_1$ orbit at the $\xi$th excited state defined by

$$\rho(j_1, \xi) = \frac{1}{k}\langle\xi|S_{j_1}^{+}\frac{\partial}{\partial S_{j_1}^{+}}|\xi\rangle \tag{66}$$

for $\xi = 1$ and $\xi = 2$. As clearly shown in Figure 2, the ground-state (the first excited state) occupation probability of the NSPM decreases (increases) with the increasing of $\mathsf{g}$ noticeably around $\mathsf{g} \sim 0.05$–$0.1$ MeV, and there is a crossing point around $\mathsf{g} \sim 0.21$ MeV. However, the occupation probability of the ground-state is always a little smaller than that of the first excited state in the SPM, which is opposite to the result of the NSPM when $\mathsf{g}$ is smaller than the value of the crossing point. They gradually decrease with the increasing of $\mathsf{g}$ with the overall pairing interaction strength fitted to the ground-state energy of the NSPM, and become close to those of the NSPM in the strong $\mathsf{g}$ limit. Therefore, the SPM is a good approximation to the NSPM only when the pairing interaction among nucleon pairs in different orbits is sufficiently strong. Nevertheless, the SPM cannot account for the actual quantum phase crossover when the pairing interaction strengths of different orbits are relatively weaker and differ

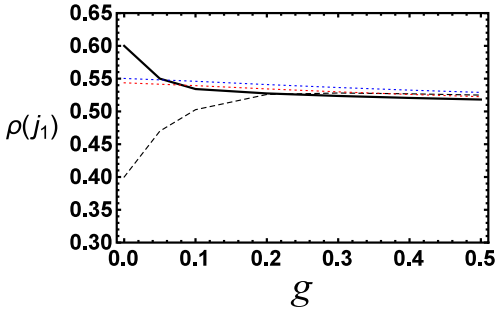


**Fig. 2.** The occupation probability of nucleon pairs in the $j_1$-orbit at the $\xi$th excited state for $\xi = 1$ and $\xi = 2$ as a function of $g_{12} = \mathrm{g}$ (in MeV) with other model parameters the same as those shown in the caption of Table 3, where the solid curve represents the occupation probability at the ground state ($\xi = 1$) of the NSPM, the dashed curve is that of the first excited state ($\xi = 2$) of the NSPM, and the dotted lines from bottom (Red) to the top (Blue) are that of the ground-state and the first excited state, respectively, in the SPM.

from those of the same orbits as required, for example, in the *ds*-shell nuclei [60]. Moreover, the on-site pairing interaction strengths $g_{t,t}$ can also change the actual ordering of the single-particle energies. For example, when $g_{2,2}$ is sufficiently greater than $g_{1,1}$, the ground state of the system may be dominated by the nucleon pairs of the $j_2$-orbit though $\epsilon_2$ is greater than $\epsilon_1$, which may be used to elucidate the inversion of the single-particle energy ordering of a shell model. Obviously, these phase transition associated issues cannot be described by the SPM, for which the NSPM should be adopted. Moreover, as shown in [62], in the general orbit-dependent pairing model [16,63], the overlaps between the exact and variationally optimized eigenstates are also large, which is in line with the observation shown above.

### 2.5 Deformed mean-field plus nearest level pairing

Within the deformed mean field, there are several types of pairing interactions that can be solved exactly. The nearest-level pairing interaction is inspired by the level-dependent Gaussian-type pairing interaction with [64]

$$G_{ii'} = -G_{\mathrm{NL}} e^{-B(\varepsilon_i - \varepsilon_{i'})^2}, \tag{67}$$

where $\{\varepsilon_i\}$ are a set of deformed single-particle energies concerned, $B = \frac{1}{2d}$ with $d = \sum_{i,i'}(\varepsilon_i - \varepsilon_{i'})^2/(p(p-1))$ according to the Gaussian distribution of deformed single-particle level energies, in which $p$ is the total number of the levels involved. As an approximation, this pairing interaction was further simplified to the nearest-level coupling [36], namely,

$$G_{ii} = -G_{\mathrm{NL}},\ G_{ii+1} = G_{i+1i} = -G_{\mathrm{NL}} e^{-B(\varepsilon_i - \varepsilon_{i+1})^2}, \tag{68}$$

where $G_{\mathrm{NL}} > 0$ is a real parameter, and $G_{ii'}$ are taken to be 0 otherwise. Hence, the deformed mean-field plus the nearest-level pairing (NLP) Hamiltonian can be expressed as [36]

$$\hat{H}_{\mathrm{NLP}} = \sum_{\rho=1}^{r} \varepsilon_{q_\rho} \hat{n}_{q_\rho} + {\sum_{i,i'}}' t_{ii'} b_i^\dagger b_{i'}, \tag{69}$$

where $t_{ii} = 2\varepsilon_i + G_{ii} = 2\varepsilon_i - G_{\rm NL}$ and $t_{ii+1} = t_{i+1i} = G_{ii+1}$ with $t_{ii'} = 0$ otherwise,

$$b_i^\dagger = a_i^\dagger a_{\bar{i}}^\dagger, \quad b_i = a_{\bar{i}} a_i, \tag{70}$$

where $a_i^\dagger$ is the $i$th level single-particle creation operator in the deformed basis, such as that of the Nilsson model, and $a_{\bar{i}}^\dagger$ the corresponding time-reversed state. The $b_i^\dagger$ and $b_i$ satisfy the following commutation relations:

$$[b_i, b_j^\dagger] = \delta_{ij}(1 - 2N_i), \quad [N_i, b_j^\dagger] = \delta_{ij} b_j^\dagger, \quad [N_i, b_j] = -\delta_{ij} b_j, \tag{71}$$

where $N_i = \frac{1}{2}(a_i^\dagger a_i + a_{\bar{i}}^\dagger a_{\bar{i}})$ is the pair number operator in the $i$th level. The eigenstates of (69) for $k$-pair excitation can be expressed as [36]

$$\begin{aligned} &|k; \xi, n_{q_1}, n_{q_2}, \ldots, n_{q_r}\rangle \\ &\quad = {\sum_{i_1 < i_2 \cdots < i_k}}' C^{(\xi)}_{i_1 i_2 \cdots i_k} b_{i_1}^\dagger b_{i_2}^\dagger \cdots b_{i_k}^\dagger |n_{q_1}, n_{q_2}, \ldots, n_{q_r}\rangle, \end{aligned} \tag{72}$$

where $n = 2k + \sum_{\rho=1}^{r} n_{q_\rho}$ is the total number of the system, $q_1, q_2, \ldots, q_r$ are the levels occupied by $r$ single particles, the prime indicates that $i_1$, $i_2$, $\ldots$, $i_k$ cannot be taken to be $q_1$, $q_2$, $\ldots$, $q_r$ in the summation, and $n_{q_\rho} = 1$ $(\rho = 1, 2, \ldots, r)$. If only even–even and odd-$A$ nuclei are treated without including broken-pair cases, $r$ is taken to be 1 for odd-$A$ nuclei, and 0 for even–even nuclei. In (72), The expansion coefficient $C^{(\xi)}_{i_1 i_2 \ldots i_k}$ is a determinant given by

$$C^{(\xi)}_{i_1 i_2 \ldots i_k} = \begin{vmatrix} g_{i_i}^{\xi_1} & g_{i_2}^{\xi_1} & \cdots & g_{i_k}^{\xi_1} \\ g_{i_i}^{\xi_2} & g_{i_2}^{\xi_2} & \cdots & g_{i_k}^{\xi_2} \\ \cdots & \cdots & \cdots & \cdots \\ g_{i_i}^{\xi_k} & g_{i_2}^{\xi_k} & \cdots & g_{i_k}^{\xi_k} \end{vmatrix}, \tag{73}$$

where $\xi = \{\xi_i\}$ is a selected set of $k$ eigenvalues of the $t$ matrix without the corresponding $r$ rows and columns, denoted as $\tilde{t}$, which can be used to distinguish the eigenstates with the same number of pairs, $k$, $g^{\xi_\mu}$ is the $\mu$th eigenvector of the $\tilde{t}$ matrix, and $E^{(\xi_\mu)}$ is the $\mu$th eigenvalue of the $\tilde{t}$-matrix, that is

$$\sum_{i'} \tilde{t}_{ii'} g_{i'}^{\xi_\mu} = E^{(\xi_\mu)} g_i^{\xi_\mu}. \tag{74}$$

Then, the excitation energies corresponding to (72) can be expressed as

$$E_k^{(\xi)} = \sum_{\rho=1}^{r} \varepsilon_{q_\rho} + \sum_{i=1}^{k} E^{(\xi_i)} \tag{75}$$

where the first sum runs over $r$ Nilsson levels each occupied by a single valence nucleon, which occurs in odd-$A$ nuclei or in broken-pair cases, the second one is a sum of $k$ different eigenvalues of the $\tilde{t}$-matrix. Obviously, $\tilde{t}$ is a $(p-r) \times (p-r)$ matrix, since those levels occupied by single valence nucleons are excluded resulting from the Pauli blocking. For even–even nuclei, the $k$-pair excitation energies are determined by the sum of $k$ different eigenvalues chosen from the $p$ eigenvalues of the $\tilde{t}$ matrix with $r = 0$, the total number of excited levels is $p!/k!(p-k)!$. While for odd-$A$ nuclei or broken-pair cases, the Nilsson level that is occupied by the single valence nucleon

should be excluded in the original $t$ matrix. In the latter case, the eigenvalue problem of (69) can be solved simply by diagonalizing the corresponding $\tilde{t}$ matrix as shown in (74) with the eigenstates and the corresponding eigen-energy given by (72) and (75), respectively.

Many ground-state quantities, such as binding energy, the even–odd mass difference, and the moment of inertia, etc. were calculated [37,38]. The binding energy of a nuclear system in the model is given by [42]

$$E = E^{(\text{core})} + E(\nu) + E(\pi), \tag{76}$$

where $E^{(\text{core})}$ is the binding energy of the core, taken to be a constant, and $E(\nu)$ and $E(\pi)$ are the ground state energy of the NLP of the neutron and the proton sector, respectively, calculated from (75). Then, the even–odd mass difference defined by

$$P(Z,N) = E(Z,N+1) + E(Z,N-1) - 2E(Z,N), \tag{77}$$

where $E(Z,N)$ is the binding energy of a nucleus with proton number $Z$ and neutron number $N$ shown in (76), were calculated. Figure 3 shows the even–odd mass differences (77) of $^{157-171}$Er, $^{159-174}$Yb, $^{223-235}$Th, and $^{226-239}$U calculated by using the NLP and compared with the corresponding experimental data, with which the pairing strength $G_{\text{NL}}$ for each nucleus was thus fixed. Once the pairing strength $G_{\text{NL}}$ for each nucleus is determined, the NLP results are used to calculate the moment of inertia of the first $2^+$ state of the even–even nuclei defined by $\Im_{\text{exp}} = 3\hbar^2/E(2_1^+)$, where $E(2_1^+)$ is experimentally observed excitation energy of the first $2^+$ state, and $\Im_{\text{exp}} = \hbar^2(2\Omega+3)/E(\Omega+2)$, where $\Omega$ is the ground-state bandhead spin with $\Omega \neq 1/2$, for the odd-$A$ nuclei [42], according to the Inglis cranking formula [65]

$$\Im_{\text{th}} = 2\hbar^2 \sum_{\xi} \frac{|\langle k;\xi|J_{x'}|k;\xi=1\rangle|^2}{E_k^{(\xi)} - E_k^{(1)}}, \tag{78}$$

where $J_{x'}$ is total angular momentum projected onto the $x'$ axis of the intrinsic frame, $|k;\xi=1\rangle$ and $|\xi\neq 1\rangle$ stand for ground and excited state calculated from the NLP, and the sum should run over all excited states with broken pairs. Since excitation energies with more than one broken pair are higher and contribute much less to the moment of inertia according to (78), only one broken pair states are considered in the calculation. It can be observed from Figure 4 that the moments of inertia of these nuclei calculated from the NLP is very close to the corresponding experimental values.

### 2.6 Deformed mean-field plus extended pairing

Based on the SPM, an extended pairing model for deformed nuclei was constructed with the Hamiltonian given by [39]

$$\begin{aligned}\hat{H} = &\sum_{i=1}^{p} \varepsilon_i n_i - G_{\text{ex}} \sum_{i,i'=1}^{p} b_i^\dagger b_{i'} \\ &- G_{\text{ex}} \sum_{\mu=2}^{\infty} \frac{1}{(\mu!)^2} \sum_{i_1\neq i_2\neq\cdots\neq i_{2\mu}} b_{i_1}^\dagger b_{i_2}^\dagger \cdots b_{i_\mu}^\dagger b_{i_{\mu+1}} b_{i_{\mu+2}} \cdots b_{i_{2\mu}},\end{aligned} \tag{79}$$

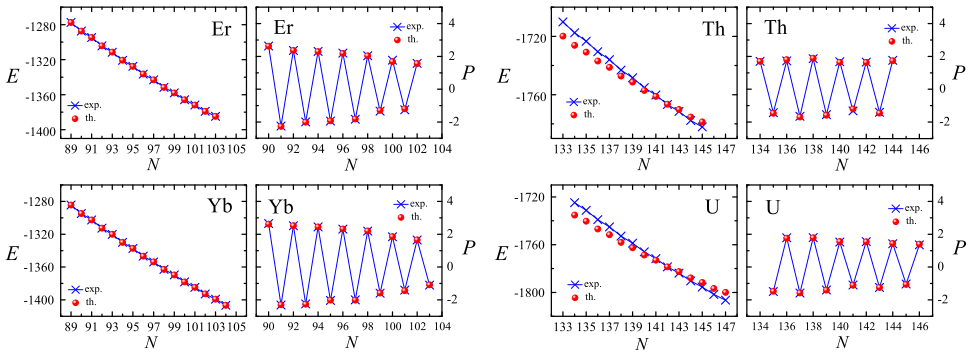


**Fig. 3.** The binding energies $E$ (in MeV) and the even–odd mass difference $P$ (in MeV) of $^{157-171}$Er, $^{159-174}$Yb, $^{223-235}$Th, and $^{226-239}$U fitted by the NLP (th.) and compared with the corresponding experimental data (exp.) taken from [66].

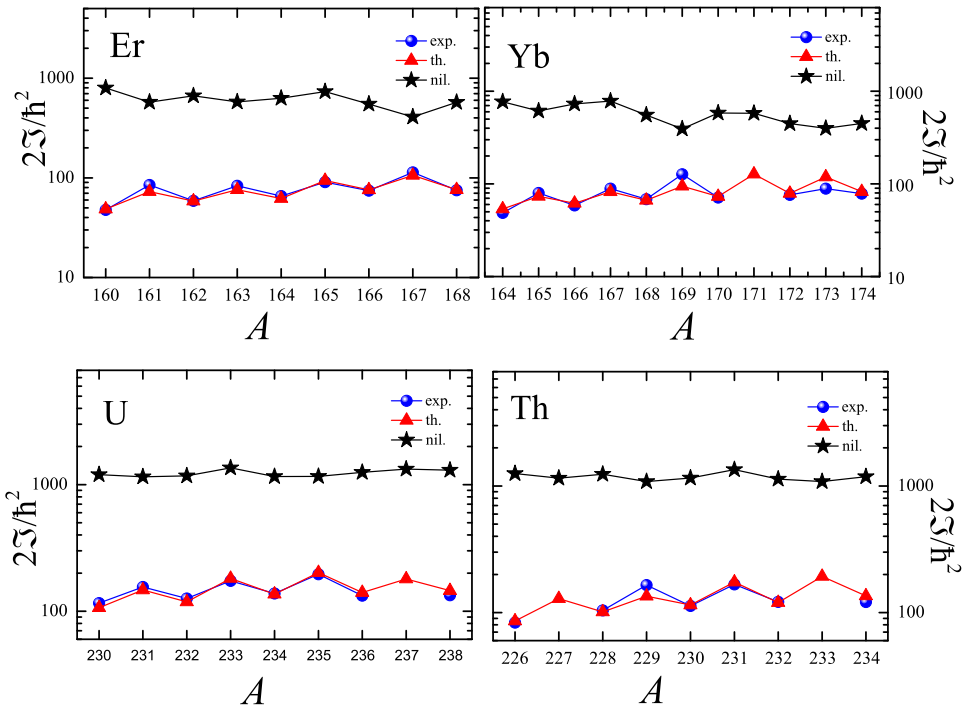


**Fig. 4.** Theoretical and experimentally deduced values related to the moment of inertia $2\Im_{\rm th}/\hbar^2$ [in $(\mathrm{MeV})^{-1}$] for $^{157-171}$Er, $^{159-174}$Yb, $^{223-235}$Th, and $^{226-239}$U, where "th." denotes theoretical results obtained from the NLP, "nil." denotes theoretical results obtained in the Nilsson mean field without pairing interaction for comparison, and the values denoted by "exp." are extracted from the experimental spectra of these nuclei [66], where $A$ is the mass number.

where $G_{\rm ex} > 0$ is the overall pairing strength. Besides the Nilsson mean-field and the standard pairing interaction, the Hamiltonian (79) also includes many-pair hopping terms that allow nucleon pairs to simultaneously scatter (hop) between and among different Nilsson levels, which is thus simply exactly solvable. Due to the Pauli exclusion, the infinite sum in (79) naturally truncates, namely, $\mu \leq [p/2]$, where $[x]$ denotes

the integer part of $x$. It is also clear that each term of the form $b_i^\dagger \cdots b_{i'}^\dagger$ and $b_l \cdots b_{l'}$ that enter into the eigenstates of (79) should have different indices $i \neq \cdots \neq i'$ and $l \neq \cdots \neq l'$.

Let $|j_1, \ldots, j_m\rangle$ be the pairing vacuum state that satisfies

$$b_i|j_1, \ldots, j_m\rangle = 0 \tag{80}$$

for $1 \leq i \leq p$, where each of the $m$ levels, $j_1, j_2, \ldots, j_m$, is occupied by a single nucleon. The $k$-pair eigenstates of (79) can be written as [39]

$$|k; \xi; j_1, \ldots, j_m\rangle = \sum_{1 \leq i_1 < i_2 < \cdots < i_k \leq p} \Lambda^{(\xi)}_{i_1 i_2 \cdots i_k} b^+_{i_1} b^+_{i_2} \cdots b^+_{i_k} |j_1, \ldots, j_m\rangle, \tag{81}$$

where $\Lambda^{(\xi)}_{i_1 i_2 \cdots i_k}$ is the expansion coefficient with

$$\Lambda^{(\xi)}_{i_1 i_2 \cdots i_k} = \frac{1}{1 - x^{(\xi)} \sum_{\mu=1}^{k} \varepsilon_{i_\mu}}, \tag{82}$$

where, similar to the results given in the Bethe ansatz approach, $x^{(\xi)}$ should satisfy

$$\frac{2}{x^{(\xi)}} + \sum_{1 \leq i_1 < i_2 < \cdots < i_k \leq p} \frac{G_{\rm ex}}{1 - x^{(\xi)} \sum_{\mu=1}^{k} \varepsilon_{i_\mu}} = 0. \tag{83}$$

The corresponding $k$-pair excitation energies are given by

$$E_k^{(\xi)} = \frac{2}{x^{(\xi)}} - G_{\rm ex}(k-1). \tag{84}$$

If only the first few eigenstates are considered, the pair structure of the eigenstates in the extended pairing model and the standard pairing model are similar, especially in the ground state. For $k$-pair excitations, $G_{\rm ex}$ in the extended pairing model and the parameter $G$ in the standard pairing Hamiltonian (3) in the deformed basis satisfy the relation [40]

$$G_{\rm ex} = ((p-k)!k!(p-k+1)k/p!)\, G. \tag{85}$$

Therefore, $G_{\rm ex}$ is very small in comparison to the standard pairing strength $G$. Once the overall pairing strength $G$ is fixed, and the parameter $G_{\rm ex}$ is chosen according to (85), it is easy to show that the difference between the ground-state energy of the extended model, $E_k^{(\rm g)}({\rm ex})$, and that of the standard pairing model in the first step approximation, $E_k^{(\rm g)}$, is given by

$$E_k^{(\rm g)}({\rm ex}) - E_k^{(\rm g)} = -(k-1)G_{\rm ex}, \tag{86}$$

which shows that the extended pairing interaction contributes a little more attraction among valence pairs than the standard pairing interaction. Since $G_{\rm ex}$ decreases drastically with increasing of $k$ toward the half-filling, the ground sate energy difference of the two Hamiltonians becomes negligible with increasing number of pairs $k$.

Since the extended pairing model can be solved exactly with a single one variable equation (83), which is simpler than the Richardson-Gaudin equations with $k$ variables shown in (11) for the standard pairing Hamiltonian in the deformed basis, the extended pairing model can be applied to relatively large systems, especially when

**Table 4.** The first pairing excitation energy (in MeV) of $^{156-164}$Er, $^{160-165}$Yb, and $^{166-168}$Hf, where only excited energies with $K = 0$ for even–even nuclei and $K = \Omega$ for odd-$A$ nuclei can be estimated from the model, the values in the $E^{\rm th}$ and $E^{\rm exp}$ columns are the calculated pairing excitation energies and the corresponding experimental values taken from [66], respectively, and the energies not experimentally available are marked by "–".

| Nucleus | $A$ | Spin and parity | $E^{\rm exp}$ | $E^{\rm th}$ |
|---|---|---|---|---|
| $^{156-164}$Er | 156 | $0_2^+$ | 0.930 | 1.360 |
| | 157 | $\frac{3}{2}_2^-$ | 0.110 | 0.444 |
| | 158 | $0_2^+$ | 0.806 | 0.886 |
| | 159 | $\frac{3}{2}_2^-$ | – | 0.231 |
| | 160 | $0_2^+$ | 0.894 | 0.476 |
| | 161 | $\frac{3}{2}_2^-$ | 0.725 | 0.375 |
| | 162 | $0_2^+$ | 1.087 | 1.264 |
| | 163 | $\frac{5}{2}_2^-$ | 0.164 | 0.359 |
| | 164 | $0_2^+$ | 1.246 | 1.870 |
| $^{160-165}$Yb | 160 | $0_2^+$ | 1.086 | 0.791 |
| | 161 | $\frac{3}{2}_2^-$ | 0.211 | 0.386 |
| | 162 | $0_2^+$ | 0.606 | 0.487 |
| | 163 | $\frac{3}{2}_2^-$ | 0.871 | 0.559 |
| | 164 | $0_2^+$ | 0.976 | 0.325 |
| | 165 | $\frac{5}{2}_2^-$ | 0.174 | 0.190 |
| $^{166-168}$Hf | 166 | $0_2{}^+$ | 0.695 | 0.387 |
| | 167 | $\frac{5}{2}_2^-$ | – | 0.106 |
| | 168 | $0_2^+$ | 0.942 | 1.298 |

only ground state and a few low-lying eigenstates, together with the corresponding eigenenergies, need to be considered. Table 4 shows the first pairing excitation energy of $^{156-164}$Er, $^{160-165}$Yb, and $^{166-168}$Hf calculated from the extended pairing model after the pairing strength $G_{\rm ex}$ for each nucleus fitted according to the even–odd mass differences [42]. Moreover, the energy ratio $R_{0_2^+/2_1^+} = (E_{0_2^+} - E_{0_g^+})/(E_{2_1^+} - E_{0_g^+})$ used to describe the evolution from vibrational to rotational shape (phase) crossover of even–even $^{156-164}$Er and $^{158-164}$Yb was also calculated [43], of which the results are shown in Figure 5.

To further explore the nature of the crossover behavior in the present model, the information (Shannon) entropy which seems suitable to reveal the crossover due to pairing interaction was also calculated [42,43]. The information entropy measures the correlations among the mean-field single-pair product states with $k$ pairs in the ground state $|{\rm g}\rangle \equiv |k;\xi = 1\rangle$ of the model, and is defined as

$$I_H(|{\rm g}\rangle) = -\sum_{i=1}^{d} |w_i|^2 \log_d(|w_i|^2), \tag{87}$$

where $\{w_i\}$ are the expansion coefficients of $|{\rm g}\rangle$ in terms of the mean-field single-pair product states, and $d$ is the dimension of the space spanned by all possible single-pair product states, namely, $k$ pairs distributed over the $p$ levels of the Nilsson mean-field. The information entropy $I_H$ varies within the closed interval $[0, 1]$. $I_H = 0$ corresponds to the ground state without the pairing interaction among valence nucleons. In this case, all valence nucleons are in the localized normal state. While $I_H = 1$ corresponds to the phase, in which the pairing interaction is extremely strong leading the ground

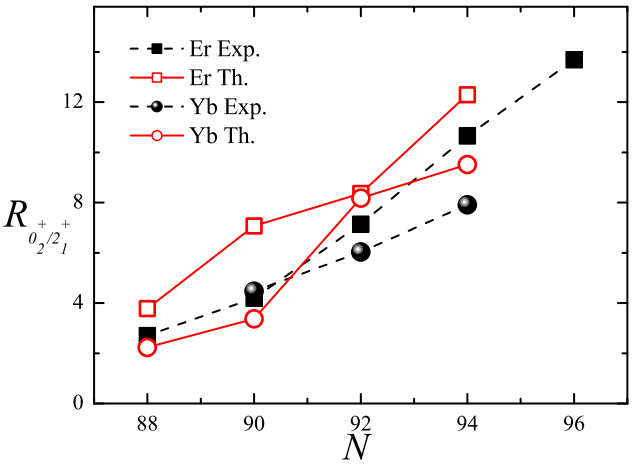


**Fig. 5.** The energy ratio $R_{0_2^+/2_1^+} = (E_{0_2^+} - E_{0_g^+})/(E_{2_1^+} - E_{0_g^+})$ of even–even $^{156-164}$Er and $^{160-164}$Yb as functions of neutron number $N$. Experimental values are denoted as "Exp.", which are taken from [66], and the values calculated from the extended pairing model are denoted as "Th.".

state to be a valence nucleon pair condensate, which is referred to as the delocalized superconducting phase. Obviously, the variation of $I_H$ as a function of the pairing interaction strength $G_{\rm ex}$ for a given value of the deformation parameter sketches the evolution from the localized normal phase towards the delocalized superconducting phase. As shown in [43], $I_H$ calculated from the extended pairing model indicates that the system undergoes the crossover from the localized normal phase with $G_{\rm ex} = 0$ and $I_H = 0$ to the delocalized superconducting (pair condensate) phase with sufficiently large $G_{\rm ex}$ and $I_H \sim 1$. Furthermore, there is also a noticeable change in the information entropy around $G_{\rm ex} \sim 0.0078 - 0.012$ MeV, which corresponds to the region where $R_{0_2^+/2_1^+}$ exhibits significant change around neutron number $N = 90$ shown in Figure 5.

## 3 Shape phase transitions in the IBM

As is well-known, the simple consistent-$Q$ formulism can be used to characterize all situations of transitional patterns in the IBM if only one- and two-body interactions are taken into consideration. The consistent-$Q$ Hamiltonian can be written as [46–48]

$$\hat{H} = c\left(\eta\,\hat{n}_d + \frac{\eta - 1}{4N}\hat{Q}(\zeta)\cdot\hat{Q}(\zeta)\right), \tag{88}$$

where $N$ is the total number of bosons in a system, $\hat{Q}(\zeta) = s^\dagger\tilde{d} + d^\dagger\tilde{s} + \zeta(d^\dagger \times \tilde{d})^{(2)}$ is the quadrupole operator, $c > 0$, $0 \le \eta \le 1$, and $-\sqrt{7}/2 \le \zeta \le \sqrt{7}/2$ are real parameters. In Figure 6, the $U(5)$ spherical shape (phase) corresponds to $\eta = 1$ case, the $O(6)$ $\gamma$-soft shape (phase) corresponds to $\eta = 0$ and $\zeta = 0$, the SU(3) prolate shape (phase) corresponds to $\eta = 0$ and $\zeta = -\sqrt{7}/2$, the $\overline{\rm SU(3)}$ oblate shape (phase) corresponds to $\eta = 0$ and $\zeta = \sqrt{7}/2$, respectively, and the $E(5)$ and the $X(5)$ or $\overline{X(5)}$ correspond to the critical symmetry points determined by the special Bohr Hamiltonian [67,68].

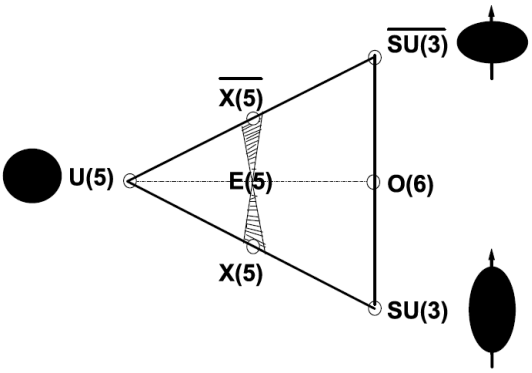


**Fig. 6.** An illustration of the extended Casten triangle.

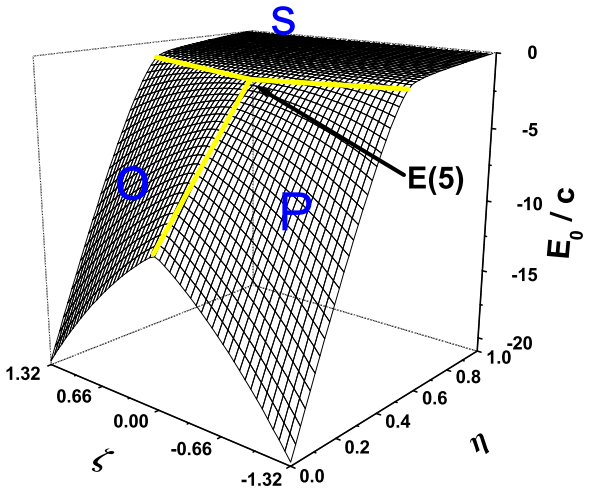


**Fig. 7.** $0_g^+$ ground-state energy $E_0/c$ as function of $\eta$ and $\zeta$ for large $N$.

Figure 7 shows the $0_g^+$ ground-state energy $E_0/c$ as function of $\eta$ and $\zeta$ for $N = 40$ bosons [69]. It can be observed from Figure 7 that the surface is symmetric with $\zeta$ reflection: $\zeta \longleftrightarrow -\zeta$, and is divided into three regions: a spherical (S) region with $\eta > 0.5$, a prolate (P) region with $\eta < 0.5$ and $\zeta < 0$, and an oblate (O) region with $\eta < 0.5$ and $\zeta > 0$. The intersection or crossing point of the lines that divide these regions is exactly the triple point corresponding to the $E(5)$ symmetry of a special Bohr Hamiltonian that describes the S, P, and O phases as existing simultaneously [70]. The dividing line between adjacent regions is rather vaguely defined for small values of $N$, but with increasing $N$ it becomes sharper and sharper. Along these lines there is a rather narrow band where the respective shapes coexist (two-phase configurations) for small values of $N$. These bands of coexisting shapes grow narrower and narrower with increasing $N$. The $0_g^+$ ground-state energy $E_0/c$ surface within these regions and the respective dividing lines are characterized in Figure 7, which agrees with the fact that the O-P, S-P, and S-O are all first order quantum phase transitions. The fact that there is a band of two-phase configurations along the lines dividing the regions appears to be a finite $N$ effect; that is, the larger the $N$ the narrower the band and the sharper the transition. These typical shape phases can be

**Table 5.** Low-lying yrast level energy ratios from the CQ-Hamiltonian in various limits.

| | U(5) | X(5) | SU(3) |
|---|---|---|---|
| | $\eta = 1$ | $\eta \sim 0.5, \zeta = -\sqrt{7}/2$ | $\eta = 0, \zeta = -\sqrt{7}/2$ |
| $E_{4_1}/E_{2_1}$ | 2.00 | 2.91 | 3.33 |
| $E_{6_1}/E_{2_1}$ | 3.00 | 5.43 | 7.00 |
| | U(5) | E(5) | O(6) |
| | $\eta = 1$ | $\eta \sim 0.5, \zeta = 0$ | $\eta = 0, \zeta = 0$ |
| $E_{4_1}/E_{2_1}$ | 2.00 | 2.20 | 2.50 |
| $E_{6_1}/E_{2_1}$ | 3.00 | 3.59 | 4.50 |

identified from the classical limit of the IBM by using the coherent state formulism [71–73].

Another quantity of the ground state is the two-neutron separation energy $S(2n)$ defined by $S(2n) = -[E_0(N-1) - E_0(N)]$, where $E_0(N)$ is the ground-state energy with $N$ bosons. In the finite-$N$ case, $S(2n)$ may be written as a smooth contribution linear with the boson number $N$ plus contribution from the deformation

$$S(2n) = -A - B\,N + S(2n)_{\rm def}\,, \tag{89}$$

where $A$ and $B$ are free parameters, of which the deformation part $S(2n)_{\rm def}$ is related to the derivative $\frac{\partial E_0}{\partial \eta}$ of the ground-state energy $E_0$ with respect to the control parameter $\eta$, and can be calculated in the classical limit with the coherent state formulism. An example is shown on the U(5)-SU(3) leg for some even–even Sm and Gd isotopes [74].

Besides the quantities of the ground state, more quantities related to some low-lying excited states are also useful to reveal the nature of quantum shape (phase) transitions in nuclei. For example, the first two energy ratios $E_{4_1}/E_{2_1}$ and $E_{6_1}/E_{2_1}$ in the yrast band shown in Table 5, which are of typical values in the vibrational $U(5)$, the rotational $SU(3)$, the $\gamma$-unstable $O(6)$ limit, and very close to the values of the $E(5)$ or the $X(5)$ critical symmetry point [67,68]. Electric quadrupole moment $Q(2_1^+)$ and some B(E2) or B(E2) ratios, where the E2 operator is taken simply as

$$\hat{T}(E2) = q_2 \hat{Q}(\zeta) \tag{90}$$

can also be adopted as an order parameter to measure the shape (phase) transitions. For example, as shown in Figure 8, $Q(2_1^+) < 0$ in the prolate ($SU(3)$ limit) case, $Q(2_1^+) = 0$ in the $\gamma$ soft ($O(6)$ limit) or spherical ($U(5)$ limit) cases, and $Q(2_1^+) > 0$ in the oblate ($\overline{SU}(3)$ limit) case. These results are consistent with the early observations made in [75,76]. Figure 9 shows $B(E2; 2_1^+ \longrightarrow 0_1^+)/q_2^2$ as a function of $\eta$ and $\zeta$ in the extended Casten triangle

The isomer shift defined by

$$\delta\langle r^2\rangle = \alpha_0 \left(\langle 2_1^+; \eta, \zeta | \widehat{n}_d | 2_1^+; \eta, \zeta\rangle - \langle 0_g^+; \eta, \zeta | \widehat{n}_d | 0_g^+; \eta, \zeta\rangle\right), \tag{91}$$

where $\alpha_0$ is a constant, is also sensitive to the transitions, which is used to define [77–79] the second order parameter $\nu_2 = \delta\langle r^2\rangle/(\alpha_0 N)$. Figure 10 displays the isomer shift in the extended Casten triangle.

In addition to the analysis of ground state properties in the extended Casten triangle, we found that the quantum phase transition behavior can also be observed in some excited states with the same angular momentum when $\eta$ and $\zeta$ assume special values. Here, we only focus on $0_2^+$ and $0_3^+$ level crossing−repulsion transition occurring

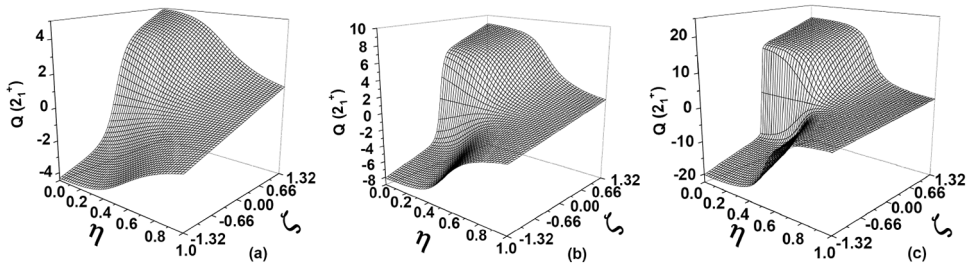


**Fig. 8.** $Q(2_1^+)$ in the unit of $q_2$ in the extended Casten triangle for $N = 5$ (a), $N = 10$ (b), and $N = 26$ (c), respectively.

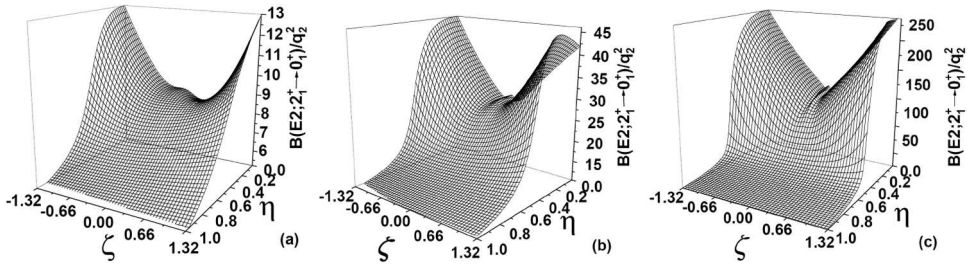


**Fig. 9.** $B(E2; 2_1^+ \longrightarrow 0_1^+)/q_2^2$ as a function of $\eta$ and $\zeta$ in the extended Casten triangle, where (a) $N = 5$, (b) $N = 10$, and (c) $N = 26$.

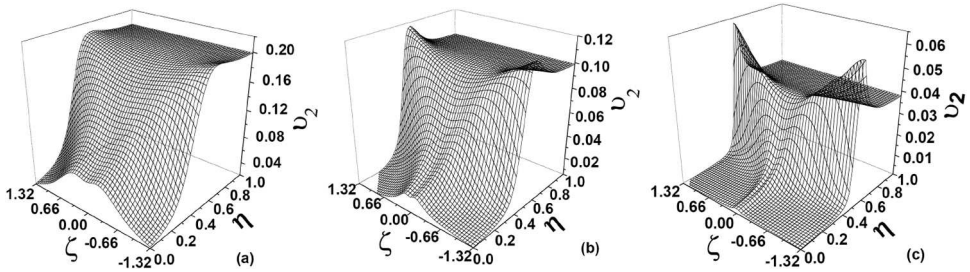


**Fig. 10.** The isomer shift $\nu_2 = \delta\langle r^2\rangle/\alpha_0 N$ as a function of $\zeta$ and $\eta$ in the extended Casten triangle for $N = 5$ (a), $N = 10$ (b), and $N = 26$ (c), respectively.

near $\eta = 0.3$ due to a change in the $\zeta$ parameter [69]. As is clearly shown on the left panel of Figure 11, there is a level crossing point near $\eta = 0.3$ when $\zeta$ is exactly zero, while it becomes level repulsion when $\zeta < 0$. The left panel of Figure 11 only shows level repulsion curves with $\zeta = -0.1$. Therefore, there is a clear $N$ independent quantum phase transition when $\zeta$ changes from $\zeta = 0$ to $\zeta < 0$. Such a quantum phase transition can also be observed from the B(E2) values associated with these two levels. The right panel of Figure 11 shows the ratios $B(E2; 0_2^+ \to 2_1^+)/B(E2; 2_1^+ \to 0_g^+)$ and $B(E2; 0_3^+ \to 2_1^+)/B(E2; 2_1^+ \to 0_g^+)$ varying with $\eta$ when $\zeta = 0$ and $\zeta = -0.1$. As can be seen, there is a clear crossing point near $\eta = 0.18$ when $\zeta = 0$, while there is no crossing when $\zeta = -0.1$. Though these ratio changes near the critical region are rather small, they can be observed for some transitional nuclei [79].

It is also shown that two-particle transfer intensities may also provide a sensitive order parameter for the shape phase transitions [80–82]. For example, the transfer

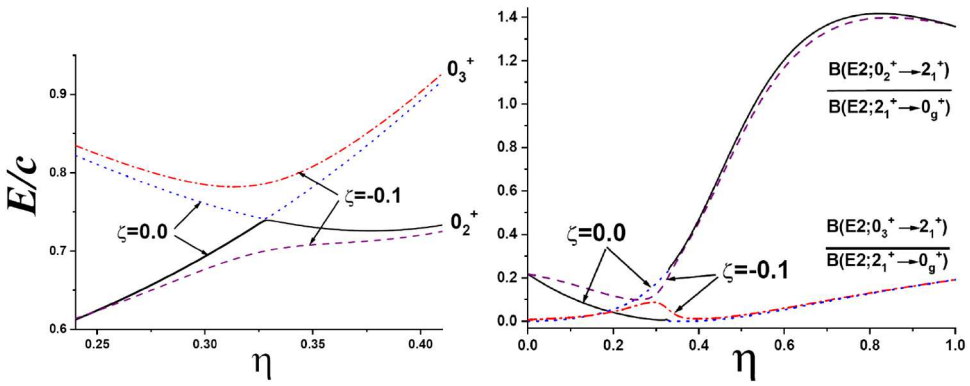


**Fig. 11.** The $0_2^+$ and $0_3^+$ level crossing−repulsion transition (left) and $B(E2;0_2^+ \to 2_1^+)/B(E2;2_1^+ \to 0_g^+)$ and $B(E2;0_3^+ \to 2_1^+)/B(E2;2_1^+ \to 0_g^+)$ as functions of $\eta$ when $\zeta = 0$, $\zeta = -0.1$ (right) with $N = 10$ bosons.

intensities defined as

$$
\begin{aligned}
I(N+1,0_1^+ \to N,0_1^+) &= |\langle N,0_1^+|s|N+1,0_1^+\rangle|^2, \\
I(N+1,0_1^+ \to N,2_1^+) &= |\langle N,2_1^+|d_0|N+1,0_1^+\rangle|^2, \\
I(N+1,0_1^+ \to N,0_2^+) &= |\langle N,0_2^+|s|N+1,0_1^+\rangle|^2
\end{aligned} \tag{92}
$$

indeed reflect the shape phase transition in some even–even Sm and Gd isotopes [81].

## 4 Summary

Recent advances in the Bethe–Richardson–Gaudin approach to various types of pairing interaction, such as the spherical mean-field plus a special separable or special non-separable pairing models, deformed mean-field plus nearest level pairing, and deformed mean-field plus extended pairing models are presented with applications to describe ground-state properties and some low-lying excitations in nuclei. Based on the Bethe–Gaudin–Richardson method, the exact solution of the standard pairing model and an effective polynomial approach to the solution are outlined. It is shown the Bethe–Gaudin–Richarson method can be generalized and extended to solve a large class of pairing problems. Exact solutions of the special separable and nonseparable pairing problems are examples of the extension. Since the pairing interaction among valence nucleons confined in a mean-field, in general, are orbit dependent, it is obvious that the special separable and nonseparable pairing interactions should be closer to the actual situations in nuclei as clearly shown in the analysis of the two-$j$ orbit case in Section 2.4. When more levels are considered, such as in the deformed mean-field case, a general level-dependent pairing interaction is not practically available. It is shown that the nearest-level pairing and the extended pairing models can be solved more efficiently than the standard pairing model with similar fitting quality to the experimental data. Finally, the shape phase transitions in the interacting boson model described by the consistent-$Q$ form with many effective order parameters (observables) to quantify the transitions are summarized.

One of the authors (F. Pan) is grateful to Professor A.K. Jain for the invitation to the SERB (DST) School on Nuclear Theory. Support from the National Natural Science

Foundation of China (11675071, 11875158, 11975009), the Liaoning Provincial Universities Overseas Training Program (2019GJWYB024), the U.S. National Science Foundation (OIA-1738287 and ACI-1713690), U.S. Department of Energy (DE-SC0005248), the Southeastern Universities Research Association, and the LSU-LNNU joint research program (9961) is acknowledged.



## References

1. A. Bohr, B.R. Mottelson, in *Nuclear structure*, (Benjamin, New York, 1969) Vol. 1: Single-particle motion
2. S.T. Belyaev, Mat. Fys. Medd. Dan. Vid. Selsk. **31** (1959)
3. P. Ring, P. Schuck, *The nuclear many-body problem* (Springer Verlag, Berlin, 1980)
4. J. Bardeen, L.N. Cooper, J.R. Schrieffer, Phys. Rev. **108**, 1175 (1957)
5. A. Bohr, B.R. Mottelson, D. Pines, Phys. Rev. **110**, 936 (1958)
6. H.C. Pradhan, Y. Nogami, J. Law, Nucl. Phys. A **201**, 357 (1973)
7. H.J. Mang, Phys. Rep. **18**, 325 (1975)
8. M. Bishari, I. Unna, A. Mann, Phys. Rev. C **3**, 1715 (1971)
9. J.Y. Zeng, C.S. Cheng, Nucl. Phys. A **405**, 1 (1983)
10. J.Y. Zeng, C.S. Cheng, Nucl. Phys. A **411**, 49 (1984)
11. H. Molique, J. Dudek, Phys. Rev. C **56**, 1795 (1997)
12. G.D. Dans, A. Klein, Phys. Rev. **143**, 735 (1966)
13. A. Covello, E. Salusti, Phys. Rev. **162**, 859 (1967)
14. A. Volya, B.A. Brown, V. Zelevinsky, Phys. Lett. B **509**, 37 (2001)
15. A.K. Kerman, R.D. Lawson, M.H. Macfarlane, Phys. Rev. **124**, 162 (1961)
16. V. Zelevinsky, A. Volya, Phys. At. Nucl. **66**, 1781 (2003)
17. R.W. Richardson, Phys. Lett. **3**, 277 (1963)
18. R.W. Richardson, Phys. Lett. **5**, 82 (1963)
19. R.W. Richardson, N. Sherman, Nucl. Phys. **52**, 221 (1964)
20. R.W. Richardson, N. Sherman, Nucl. Phys. **52**, 253 (1964)
21. M. Gaudin, J. Phys. **37**, 1087 (1976)
22. F. Pan, J.P. Draayer, W.E. Ormand, Phys. Lett. B **422**, 1 (1998)
23. J. Dukelsky, C. Esebbag, P. Schuck, Phys. Rev. Lett. **87**, 066403 (2001)
24. J. Dukelsky, C. Esebbag, S. Pittel, Phys. Rev. Lett. **88**, 062501 (2002)
25. H.-Q. Zhou, J. Links, R.H. McKenzie, M.D. Gould, Phys. Rev. B **65**, 060502(R) (2002)
26. F. Pan, J.P. Draayer, Phys. Rev. C **66**, 044314 (2002)
27. S. Rombouts, D. Van Neck, J. Dukelsky, Phys. Rev. C **69**, 061303(R) (2004)
28. J. Dukelsky, S. Pittel, G. Sierra, Rev. Mod. Phys. **76**, 643 (2004)
29. G. Ortiz, R. Somma, J. Dukelsky, S. Rombouts, Nucl. Phys. B **707**, 421 (2005)
30. J. Dukelsky, V.G. Gueorguiev, P. Van Isacker, S. Dimitrova, B. Errea, S. Lerma H., Phys. Rev. Lett. **96**, 072503 (2006)
31. A.B. Balantekin, J.H. de Jesus, Y. Pehlivan, Phys. Rev. C **75**, 064304 (2007)
32. A.B. Balantekin, Y. Pehlivan, Phys. Rev. C **76**, 051001(R) (2007)
33. F. Pan, L. Bao, L. Zhai, X. Cui, J.P. Draayer, J. Phys. A: Math. Theor. **44**, 395305 (2011)
34. X. Guan, K.D. Launey, M. Xie, L. Bao, F. Pan, J.P. Draayer, Phys. Rev. C **86**, 024313 (2012)
35. X. Guan, K.D. Launey, M. Xie, L. Bao, F. Pan, J.P. Draayer, Comp. Phys. Commun. **185**, 2714 (2014)
36. F. Pan, J.P. Draayer, J. Phys. A: Math. Gen. **33**, 9095 (2000)
37. Y. Chen, F. Pan, G.S. Stoitcheva, J.P. Draayer, Int. J. Mod. Phys. B **16**, 2071 (2002)

38. F. Pan, Y. Wang, X. Guan, J. Lu, X.-R. Chen, J.P. Draayer, AIP Conf. Proc. **1342**, 63 (2011)
39. F. Pan, V.G. Gueorguiev, J.P. Draayer, Phys. Rev. Lett. **92**, 112503 (2004)
40. F. Pan, M.-X. Xie, X. Guan, L.-R. Dai, J.P. Draayer, Phys. Rev. C **80**, 044306 (2009)
41. X. Guan, H. Li, Q. Tan, F. Pan, J.P. Draayer, Chin. Phys. C **35**, 747 (2011)
42. X. Guan, K.D. Launey, Y. Wang, F. Pan, J.P. Draayer, Phys. Rev. C **92**, 044303 (2015)
43. X. Guan, H. Zhao, F. Pan, J.P. Draayer, Nucl. Phys. A **986**, 86 (2019)
44. S. Sachdev, *Quantum phase transitions* (Cambridge University Press, Cambridge, England, 1999)
45. A. Bohr, B.R. Mottelson, in *Nuclear structure* (World Scientific, Singapore, 1998), Vol. 2
46. F. Iachello, A. Arima, *The interacting boson model* (Cambridge University, Cambridge, England, 1987)
47. P. Cejnar, J. Jolie, Prog. Part. Nucl. Phys. **62**, 210 (2009)
48. P. Cejnar, J. Jolie, R.F. Casten, Rev. Mod. Phys. **82**, 2155 (2010)
49. K. Heyde, P. Van Isacker, M. Waroquier, J.L. Wood, R.A. Meyer, Phys. Rep. **102**, 291 (1983)
50. J.L. Wood, K. Heyde, W. Nazarewicz, M. Huyse, P. Van Duppen, Phys. Rep. **215**, 101 (1992)
51. K. Heyde, J.L. Wood, Rev. Mod. Phys. **83**, 1467 (2011)
52. F. Pan, J.P. Draayer, Nucl. Phys. A **636**, 156 (1998)
53. G. Szegö, in *Amer. Math. Soc. Colloq. Publ.* (American Mathematical Society, Providence, RI, 1975), Vol. 23
54. X. Guan, K.D. Launey, J. Gu, F. Pan, J.P. Draayer, Phys. Rev. C **88**, 044325 (2013)
55. F. Pan, D. Zhou, L. Dai, J.P. Draayer, Phys. Rev. C **95**, 034308 (2017)
56. L. Dai, F. Pan, J.P. Draayer, Nucl. Phys. A **957**, 51 (2017)
57. S.M.A. Rombouts, J. Dukelsky, G. Ortiz, Phys. Rev. B **82**, 224510 (2010)
58. P.W. Claeys, S. De Baerdemacker, M. Van Raemdonck, D. Van Neck, Phys. Rev. B **91**, 155102 (2015)
59. F. Pan, D. Zhou, Y. He, S. Yang, Y. Zhang, J.P. Draayer, Phys. Lett. B **795**, 165 (2019)
60. F. Nowacki, A. Poves, Phys. Rev. C **79**, 014310 (2009)
61. F. Pan, S. Yuan, Y. He, Y. Zhang, S. Yang, J.P. Draayer, Nucl. Phys. A **984**, 68 (2019)
62. S. De Baerdemacker, P.W. Claeys, J. Caux, D. Van Neck, P.W. Ayers, arXiv:1712.01673 (2017)
63. A. Holt, T. Engeland, M. Hjorth-Jensen, E. Osnes, Nucl. Phys. A **634**, 41 (1998)
64. H. Molique, J. Dudek, Phys. Rev. C **56**, 1795 (1997)
65. D.R. Inglis, Phys. Rev. **96**, 1059 (1954)
66. A.K. Jain, R.K. Sheline, P.C. Sood, K. Jain, Rev. Mod. Phys. **62**, 393 (1990)
67. F. Iachello, Phys. Rev. Lett. **85**, 3580 (2000)
68. F. Iachello, Phys. Rev. Lett. **87**, 052502 (2001)
69. F. Pan, T. Wang, Y.-S. Huo, J.P. Draayer, J. Phys. G **35**, 125105 (2008)
70. D.D. Warner, Nature **420**, 614 (2002)
71. J.N. Ginocchio, M.W. Kirson, Nucl. Phys. A **350**, 31 (1980)
72. A.E.L. Dieperink, O. Scholten, F. Iachello, Phys. Rev. Lett. **44**, 1747 (1980)
73. P. Van Isacker, J.-Q. Chen, Phys. Rev. C **24**, 684 (1981)
74. Y. Zhang, F. Pan, Y.-X. Liu, Y.-A. Luo, J.P. Draayer, Phys. Rev. C **88**, 014304 (2013)
75. P. Cejnar, S. Heinze, J. Jolie, Phys. Rev. C **68**, 034326 (2003)
76. J. Jolie, A. Linnemann, Phys. Rev. C **68**, 031301(R) (2003)
77. F. Iachello, N.V. Zamfir, R.F. Casten, Phys. Rev. Lett. **81**, 1191 (1998)
78. F. Iachello, N.V. Zamfir, Phys. Rev. Lett. **92**, 212501 (2004)
79. F. Pan, Y. Zhang, J.P. Draayer, J. Phys. G: Nucl. Part. Phys. **31**, 1039 (2005)
80. R. Fossion, C.E. Alonso, J.M. Arias, L. Fortunato, A. Vitturi, Phys. Rev. C **76**, 014316 (2007)
81. Y. Zhang, F. Iachello, Phys. Rev. C **95**, 034306 (2017)
82. K. Nomura, Y. Zhang, Phys. Rev. C **99**, 024324 (2019)